Comparative energy, exergy, economic, and environmental (4E) analysis and optimization of two high-temperature Kalina cycles integrated with thermoelectric generators for waste heat recovery from a diesel engine

Arvin Sohrabi [a], Nima Asgari [b], Muhammad Imran [c,*,1], Muhammad Wakil Shahzad [d,*,1]

[a] *School of Mechanical Engineering, Beijing Institute of Technology, Beijing 100081, China*
[b] *Department of Electrical & Computer Engineering, Western University, ON, Canada*
[c] *Department of Mechanical, Biomedical and Design Engineering, Aston University, B4 7ET Birmingham, UK*
[d] *Department of Mechanical and Construction Engineering, Northumbria University, Newcastle Upon Tyne NE1 8ST, UK*

ARTICLE INFO

ABSTRACT

High-temperature Kalina cycles are among the efficient approaches to recovering waste heat. However, high-temperature Kalina cycles are characterized by complex layouts, lower efficiency, and higher cost. This work aims at conducting a comparative thermodynamic, economic, and environmental assessment of two different configurations of the high-temperature Kalina cycle. Thermoelectric generators, as the simple and developing heat recovery modules for electricity generation, have been embedded in the condensers of the simple High-temperature Kalina cycle, thereby proposing the enhanced thermal performance of the Kalina cycles. A parametric optimization approach was adopted to optimize the net power output and the location of pinch points of condensers. The results indicate that thermoelectric generators can improve the total power capacity of High-temperature Kalina cycles by about 0.29–0.82 kW. Meanwhile, the economic feasibility of this integration has also been investigated. The first enhanced Kalina cycle has energy and exergy efficiencies of 32 % and 63.23 %, respectively. As an economic parameter, the net present values of these cycles are 84.56, 84.77, 86.63, and 86.84 k$ for standard Kalina cycle configuration 1, enhanced Kalina cycle configuration 1, standard Kalina cycle configuration 2, and enhanced Kalina cycle configuration 2, respectively. In addition, the environmental assessment reveals that 15.55, 15.85, 15.54, and 15.84 lit/hr diesel fuel would be saved by operating the waste heat recovery cycles, respectively. Finally, a parametric study has been carried out to study the influences of variations of different parameters on the performance criteria of all four cycles.

1. Introduction

It is evident that the utilization of fossil fuels, thereby accumulation of CO_2 in Earth's atmosphere, causes severe environmental consequences, including global warming and climate change [1]. About 60–70 % of the total fossil fuel consumption of an industrial country is attributed to internal combustion engines (ICEs) [2]. About 50–60 % of the input fuel energy in ICEs is discarded into the environment as waste, and exhaust gases have a significant amount of thermal energy [3]. In addition to all the technological and environmentally friendly advancements that have taken place in this area, waste heat recovery (WHR) from internal combustion engines is an undisputedly efficient strategy to improve the efficiency of ICEs. It leads to more power/energy production without burning excess fossil fuel. Thermodynamic cycles, especially those working with organic fluids (e.g., organic Rankine cycle (ORC) [4]) and Kalina cycle (KC) [5], are the best choice for converting the waste heat to electricity and improving the efficiency of the whole system [6]. Countless studies have been conducted in the literature aiming at thermodynamic analysis of ORC and KC as the WHR systems of ICEs.

Four different configurations of ORC-based WHR systems were introduced and assessed from the thermodynamic and economic viewpoints by Simone Lion et al. [7] in order to exploit the maximum waste thermal energy of a two-stroke marine Diesel engine. The R1233zd(E) was the best choice among the working fluids, and the fuel economic benefits of 5.4 % and 5.9 % were found for Tier II and III operation modes at full load. Mohammadkhani and Yari [8] employed a

---

* Corresponding authors.
  E-mail addresses: m.imran12@aston.ac.uk (M. Imran), muhammad.w.shahzad@northumbria.ac.uk (M. Wakil Shahzad).
[1] The two authors have the same contribution to this study.

Nomenclature

Abbreviations

SKC	Simple Kalina Cycle
EKC	Enhanced Kalina Cycle
TEG	Thermoelectric Generator
ICE	Internal Combustion Engine
WHR	Waste Heat Recovery
KC	Kalina Cycle
ORC	Organic Rankine Cycle
CCHP	Combined Cooling, Heating and Power
CHP	Combined Heat and Power
MX	Mixing Chamber
TE	Thermoelectric
CI	Capital Investment
OM	Operation and Maintenance
SPECO	Specific Exergy Costing
SQP	Sequential Quadratic Programming

Symbols

A	Area (m^2)
AP	Annual profit (k$)
C	Cost ($)
c	Unit price of energy ($/kWh)
$\dot{C}$	Cost rate ($ s^{-1})
CELF	Constant escalation levelization factor
CF	Capacity factor
CRF	Capital recovery factor
e	Specific exergy (kJ kg^{-1})
$\dot{E}$	Exergy rate (kW)
FCI	Fixed capital investment (k$)
h	Specific enthalpy (kJ kg^{-1})
$\dot{H}$	Enthalpy rate (kW)
i	Interest rate
LC	Levelized cost of electricity ($/MJ)
LT	Lifetime (year)
$\dot{m}$	Mass flow rate (kg s^{-1})
P	Pressure (kPa, bar)
PC	Purchased equipment cost (k$)
PP	Payback period
PV	Net present value (k$)
Q	Quality
$\dot{Q}$	Heat rate (kW)
r	Inflation rate
s	Specific entropy (kJ kg^{-1} K^{-1})

T	Temperature (°C)
t	Time (year)
TI	Total capital investment (k$)
U	heat transfer coefficient (W m^{-2} K^{-1})
$\dot{W}$	Power (kW)
x	Ammonia concentration
Y	Cost coefficient
Z	Figure of merit
z	Decision variable

Subscripts

0	Ambient conditions
AV	Avoided
c	Cold
CD	Condenser
CW	Cooling water
D	Destruction
en	Energy
ex	Exergy
F	Fuel
h	Hot
HX	Heat exchanger
in	Input
m	mean
MX	mixing chamber
net	network
out	Output
P	Product
PP	Pinch point
Pu	Pump
Re	Recuperator
se	Sold electiricty
Sep	Separator
SG	Steam generator
SV	Saved
Tu	Turbine
TV	Throttling valve
wf	Working fluid

Greek letter

Σ	Summation
η	Efficiency (%)
Δ	Difference indicator
τ	Tax rate

transcritical dual-loop ORC to utilize the waste heat from a turbocharged diesel engine's exhaust gas and coolant. Using toluene and R143a as working fluids for the HT and LT loops, respectively, their results indicated a thermal efficiency equal to 20.63 % and 9.2 years for the payback period. Jafarzad et al. [9] showed that the direct utilization of waste heat from a turbocharged marine Diesel engine's exhaust gas maximized the exergy efficiency of the combined heat and power (CHP) system while employing the ORC as the WHR cycle. Sohrabi et al. [10] revealed that using the zeotropic mixtures in ORCs can improve the cycle performance and reduce its exergy destruction owing to the difference in these mixtures' boiling and condensation temperature. This is one of the reasons making the Kalina cycle show a better thermal matching within the evaporator and condenser since the mixture of water-ammonia is usually used as the working fluid in KC [11]. Other studies have also been conducted to evaluate the pros and cons of ORC and KC, the most significant results of which are briefly presented in Table 1:

Accordingly, researchers have appropriately studied the thermodynamic and economic aspects of applying the Kalina cycle in WHR applications from ICEs. Also, the high-temperature Kalina cycle has been used commonly for the utilization of high-temperature waste heat in industry or from ICEs due to its higher efficiency compared to the other conventional Kalina cycles. One of the primary comprehensive assessments of the thermodynamic performance of a simplified high-temperature Kalina cycle (as a bottoming cycle) was carried out by C. H. Marston in 1990 [19]. It was expressed that the turbine inlet composition and the separator temperature are the most important parameters in optimizing the performance of the KC. Modi and Haglind [20] conducted a thermodynamic analysis and optimization on four different configurations of high-temperature KC with the aim of increasing their efficiencies. The turbine inlet temperature of these cycles can reach up to 500 °C. The decision variables in their optimization problem were the turbine outlet pressure, the separator inlet temperature, and the separator inlet ammonia mass fraction. The most complex

Table 1

The most important results and conclusions of studies on the thermodynamic and thermo-economic performance of ORCs and KCs.

Reference	Evaluation	Significant results
Bombarda et al. [12]	Thermodynamic comparison between the KC and ORC in WHR from 8900 kWe Diesel engines.	The power generation capacity of KC was 0.7 % higher than ORC; The maximum pressure of KC was 10 times higher than that of the ORC.
Nemati et al. [13]	Thermodynamic comparison between the KC and ORC in WHR from a gas turbine-based cogeneration system.	The turbine size parameter for KC was lower than that of the ORC.
Milani et al. [14]	Optimization problem on different ORC/Kalina-based systems for WHR from a gas engine.	The least important variables from the viewpoint of efficiency were the KC and ORC pump isentropic efficiency and ammonia/water concentration in the KC.
Feng et al. [15]	A comprehensive parametric study on the thermodynamic performance of a combined supercritical CO_2 Bryton cycle and KC.	Reducing the outlet temperature of the KC condenser caused a reduction in the net power output.
Ding et al. [16]	Running the evaporator of a KC and a humidification-dehumidification (HDH) desalination cycle, respectively by the exhaust gas and the jacket water of a low-temperature diesel engine.	Increasing the basic ammonia concentration had a negative impact on the performance of the whole system. The system's energy and exergy efficiencies were enhanced by 1.88 % and 1.52 %, and sum unit of cost of product (SUCP) was decreased by 0.94 \$/GJ after the optimization.
Mao et al. [17]	A system composed of dual pressure KC and HDH cycle was investigated in terms of energy, exergy, and exergoeconomics.	Increasing the pinch point temperature difference of the KC's vapor generator (evaporator), the inlet pressure of the turbine, and the basic ammonia concentration led to undesirable outcomes in the overall system performance; The maximum exergy destruction rate with the value of 39.88 kW occurred in the condenser.
Shokri Kalan et al. [18]	A novel combined cooling and power (CCP) system, in which a KC and a double-effect absorption chiller were driven by the exhaust gas of an ICE, was proposed.	The boiler, the turbine, and the distillation column had the highest exergy destruction rate, respectively. The costs related to the exergy destruction in the boiler, recuperators, and turbine were higher than their investment costs.

layout (KC1234) and KC123 had the highest electrical efficiencies of 31.47 % and 31.46 %, respectively. The lowest efficiency was related to the basic high-temperature configuration (KC234) proposed by C. H. Marston [14].

Sohrabi and Behbahaninia [21] chose one of the high-temperature Kalina cycles of Modi and Haglind [20] and a simple ORC to recover the waste heat of a Diesel engine. Based on the results of the advanced exergy and exergoeconomic analyses, it was found that the total exergy destruction of the WHR system was 44 kW, 27 % of which was attributed to the Kalina steam generator. Moreover, the unavoidable cost rates are the majority for most components of the system. Mohammadkhani et al. [22] made a modification in the structure of the high-temperature KC (KC12 proposed by Modi and Haglind [20]) by directing a Diesel engine's coolant water to the Kalina cycle's preheater, while the exhaust gas of the engine operated as the main heat source. The proposed KC could produce 21.74 kW of power in addition to the engine capacity of 98.9 kW. The exergoeconomic analysis demonstrated that the unit cost of KC turbine output power is 15.52 $cent/kWh$.

According to the energy crisis growing with the world's population growth and replacing conventional mechanical devices with electrical ones, and regarding the net zero goal in 2050, it is necessary to increase the electricity production capacity by about half of the current total energy consumption [23]. Therefore, attempting to produce more electricity besides enhancing the efficiency of power generation technologies would help us overcome the above-mentioned crisis. One of the simple and developing devices for the efficiency enhancement of thermal power cycles, which has gained massive traction in recent decades, is the thermoelectric generator (TEG). From the thermodynamic

perspective, TEG is a heat engine working between a heat source and a heat sink, producing electromotive force due to temperature differences [23]. TEGs consist of simple thermoelectric (TE) modules that can be inserted inside a heat exchanger to drive them with the temperature difference between two streams and reduce the excess costs of building new heat exchangers.

Deployment of TEG in energy conversion systems has been gained attention in recent years, and consequently, researchers attempted to investigate the pros and cons of its application in various WHR systems, as listed in Table 2.

Furthermore, it is also practical to benefit TEGs inside heat exchangers with a phase-changing process. The most rational application is the condenser since usually the cooling stream of the condenser does not have a practical use, so there is no limitation in how much heat can be obtained by the cooling stream and how much can be led to TEG. This has been applied in the Kalina cycle by Malik et al. [29] and Musharavati et al. [30]. Malik et al. [29] compared the exergetic performances of three Kalina-based combined cooling, heating and power (CCHP) systems, including basic KC, KC integrated with TEG, and KC integrated with TEG and PEM Fuel Cell (PEMFC). Based on their investigations, embedding the TEG module in the condenser of the Kalina cycle improved the system's energy and exergy efficiency by 1.7 % and 5.7 %, respectively. The results of a 3E assessment on the CCHP/TEG system composed of ORC, KC, and Steam cycle revealed that TEG is among the top four components with the highest exergy destruction rate, according to Musharavati et al. [30]. They concluded that increasing the maximum temperature and the maximum pressure of the Kalina cycle, respectively, have a positive and negative effect on the net power output of the

Table 2

The most important results and conclusions of studies on the thermodynamic aspects of deployment of TEGs in various energy conversion systems.

| Reference	Evaluation	Significant results
Mahmoudan et al. [24]	3E analyses and multi-objective optimization of a multi-generation system integrated with TEG.	An acceptable enhancement in total power generation and the levelized cost of electricity (LC) of the cycle could be achieved by using TEG.
Malik et al. [25]	Evaluating the impact of TEG on the performance of the ocean thermal energy conversion (OTEC) system composed of an ORC and a proton exchange membrane electrolyzer (PEME).	Applying TEG in this system brought about up to 7.2 % excess H_2 production.
Nabat et al. [26]	Used a TEG inside the hot oil cooler in their Compressed Air Energy Storage system (CAES).	They could produce 13.82 kW excess power.
Zhang et al. [27]	Energy and exergy efficiency of three combined cycles with topping cycles of steam Rankine, Bryton, and TEG and the bottoming cycle of ORC have been assessed.	TEG-ORC system showed limited energy exploitation performance.
Zare and Palideh [28]	Employed TEG to recover the waste heat of a Kalina cycle's condenser indirectly.	Increasing the ammonia mass fraction caused an increase in the power output of the TEG; The output power of TEG was sufficient to be used by both cycle pumps.
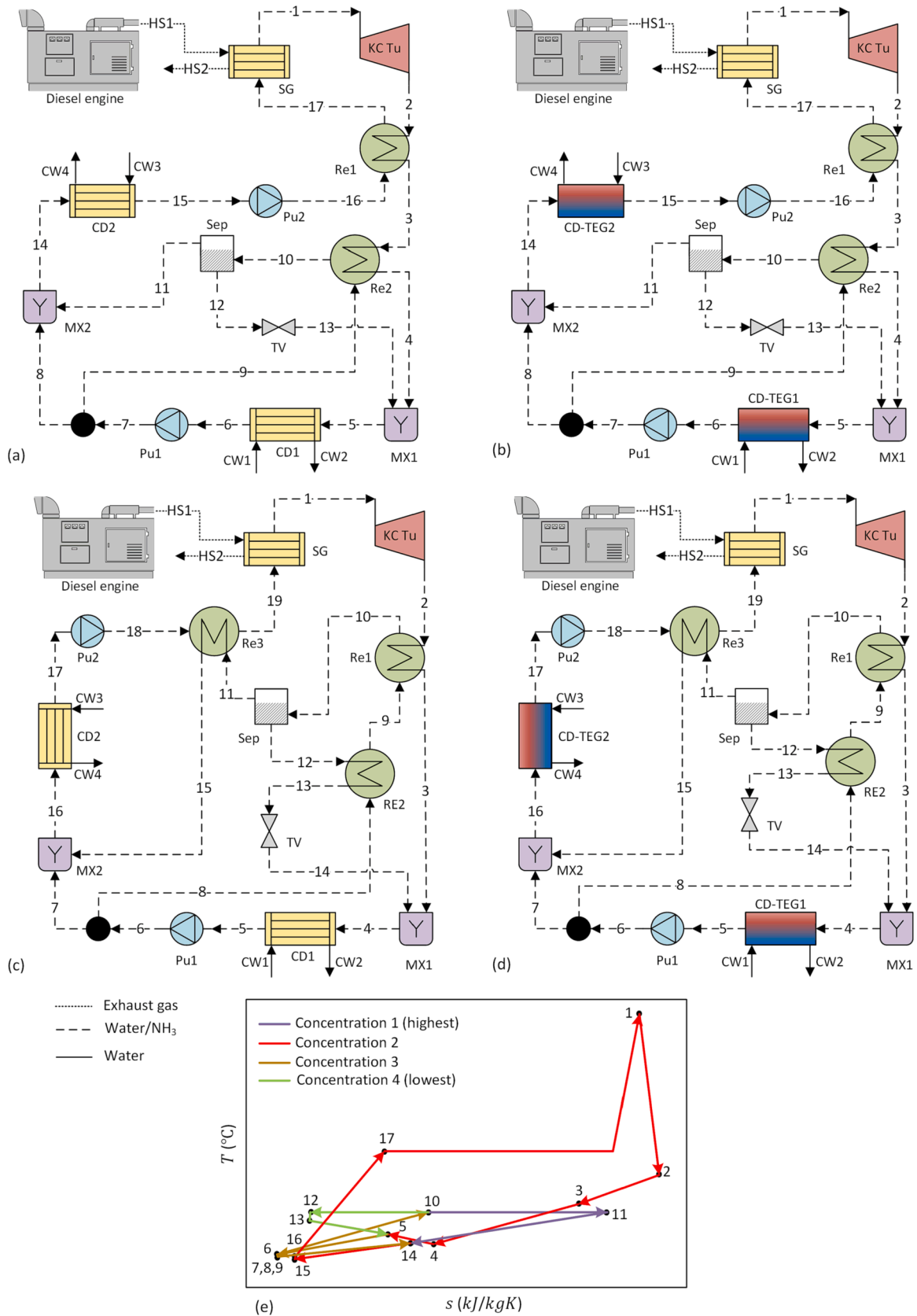
Fig. 1. The schematic of the proposed Kalina cycles for waste heat recovery from the Diesel engine; (a) SKC1 (b) EKC1 (c) SKC2 (d) EKC2 (e) the T-s diagram of the SKC1.

Table 3

Description of two High-temperature Kalina cycles and their enhanced forms, studied in the present work.

Structure	Description
SKC1	This is the simplest high-temperature Kalina cycle. It was first introduced by Marston [19] and includes two internal heat exchangers to recover more heat for high-temperature applications (Re1 and Re2). These recuperators are used to recover the available heat in the turbine outlet stream.
EKC1	It is a modified form of SKC1, with TEG modules integrated into the condensers for more power generation.
SKC2	This structure is introduced and discussed in [20]. It features one more internal recuperator compared to SKC1 for more heat recovery within the cycle (Re3). This recuperator preheats the working fluid before the steam generator utilizing the available heat in the separator outlet stream.
EKC2	This structure enhances the SKC2 by merging TEG modules into the two condensers

system. After optimization, the best operation point of the total system was where the exergy efficiency and the electrical cost rate were 22.11 % and 12.52 $/h$, respectively.

It can be concluded that researchers have studied the WHR and combined utilization potentials of Kalina cycles in terms of energy and exergy. Also, the application of TEGs in performance enhancement of the Kalina-based systems has been evaluated in some research papers from the exergoeconomic perspective. However, there are still some research gaps and open questions in the literature, which are addressed in this work and can be considered as the novelty of the present study. These include.

Two basic and well-known configurations of the high-temperature Kalina cycle (proposed in [19;20]) have been analyzed in terms of energy and exergy by other researchers. However, conducting comparative economic and environmental evaluations on these two KCs is highly required in the literature.

The thermodynamic and economic feasibility of performance improvement of the two mentioned high-temperature Kalina cycles with thermoelectric generators has been studied in this research for the first time.

Limited studies have taken place regarding the thermal and economic feasibility analysis of the deployment of TEGs in industrial power cycles, which makes the researchers tentative about the integration of TEGs with the energy provision sectors. Unfortunately, several articles have used incorrect equations for calculating the efficiency of TEG based on the definition of the first law of thermodynamics, or their authors have used unreliable values for TEG's figure of merit (Z) without providing authentic references and enough discussion on these values. Meanwhile, in some other cases, the TEG model has not been validated against the results of other references. This work, however, aims to use the most reliable sources for the thermodynamic modeling of TEGs and the assumptions used in the model.

The energy modeling of the Kalina cycles follows a self-optimized procedure. This procedure is to maximize the net output power of cycles. The main effort in this section goes to finding a new way of optimization that speeds up the procedure compared to the previous works.

The present work aims to conduct a comparative thermodynamic, economic, and environmental assessment of two high-temperature Kalina cycles and their enhanced forms employing TEGs (4 cycles). These two high-temperature cycles have been selected due to their relatively simple composition compared to the other high-temperature KCs. In the integrated form of the Kalina cycles, TEGs have been embedded in the condensers (two TEGs for each KC). The waste heat of a Diesel engine's exhaust gas is the heat source of these cycles. Hence, the WHR potentials of all the simple and enhanced KCs are investigated in this work. All these cycles are modeled, evaluated, and optimized in MATLAB simulation environment, considering the net power output as the objective function. It is also worth noting that one of the selected simple Kalina cycles has been investigated considering the advanced

Table 4

The characteristics of the considered Diesel engine [10].

Characteristic	Value
Model name	C13 ACERT-DE400E0
Nominal capacity	400 kVA
Power factor	0.8
Generated power	320 kW
Fuel consumption	83.5 L/hr
Exhaust gas temperature	529.2 $°C$
Exhaust gas flow rate	62.8 m^3/min (0.447 kg/s)

exergy and exergo-economic approaches in our previous work [21].

2. System description

This study attempts to recover the heat rejected from a Diesel engine's exhaust gas using two different Kalina cycles and their enhanced configurations. The enhanced forms include TEGs that are inserted in the condensers. The four systems' schemas are illustrated in Fig. 1, and their descriptions are provided in Table 3. These systems are described in detail in Sections 2.2 and 2.3, as well.

2.1. Heat source (A 320 kW Diesel engine's exhaust gas)

The engine selected to study in this work is the same engine chosen as the waste heat source in our previous article [21]. However, since the thermal energy of the engine's jacket water was not comparable with that of the exhaust gas, in this study, the engine's exhaust gas is the only waste thermal energy source to be recovered by the bottoming Kalina cycles. The technical characteristics of the considered engine are presented in Table 4 [10]. The composition of the engine's exhaust gas is obtained from Ref. [21]: $N_2 = 0.7642, O_2 = 0.0948, CO_2 = 0.0756$, and $H_2O = 0.0654$.

2.2. The first Kalina cycle (SKC1 and EKC1)

Fig. 1 (a) presents the first configuration of the simple Kalina cycle (SKC1). The working fluid (the ammonia-water solution) receives the waste heat of the engine's exhaust gas and starts to evaporate through a steam generator (SG). Stream 1, with the ammonia mass fraction of 0.7, enters the KC turbine and, after expansion, passes through the recuperator 1 (Re1) to preheat the inlet stream of SG. Again, the low-pressure vapor (stream 3) flows through the recuperator 2 (Re2) to conduct its thermal energy to the basic solution. Then, it is directed to mixing chamber 1 (MX1) to blend with the lean saturated solution coming from the separator and throttle valve (stream 13) and make up the lean vapor on point 5. After being pumped, the condensed working fluid (stream 6) is directed to the splitter, where it is divided into streams 8 and 9. Stream 8 is mixed with the rich vapor, detached from the saturated basic solution (stream 10) in the separator, to reproduce the vapor fluid with a mass fraction of 0.7 (stream 14).

This solution enters the second condenser (CD2), and after condensation, its pressure is increased to the maximum pressure of the cycle by passing through pump 2. Finally, stream 16 gets ready to reenter the steam generator after being preheated in Re1. The integrated or thermally enhanced KC (EKC1), presented in Fig. 1 (b), includes two CD-TEGs. A TEG is embedded in each condenser to produce excess electrical power using the thermal energy transferred through it.

2.3. The second Kalina cycle (SKC2 and EKC2)

The major difference between this structure and the first one is the number of recuperators and their locations in the cycle. Fig. 1 (c) schematically illustrates the simple Kalina cycle 2 (SKC2). First, the stream separated from the splitter (stream 8) is preheated twice: first, by passing through Re2 and getting the thermal energy of lean solution

Table 5
Thermodynamic assumptions for the modeling and optimization process [20,22,31].

Parameter	Value
Ambient temperature ($^\circ C$)	30
Ambient pressure (*bar*)	1.013
Heat source (exhaust gas) minimum temperature ($^\circ C$)	120
Heat source pressure (*bar*)	1.013
Cooling water inlet temperature ($^\circ C$)	20
Cooling water outlet temperature ($^\circ C$)	30
Cooling water pressure (*bar*)	1.013
Pump isentropic efficiency (%)	70
Turbine isentropic efficiency (%)	85
Steam generator PP temperature ($^\circ C$)	15
Other heat exchangers PP temperature ($^\circ C$)	7
Turbine inlet Ammonia concentration	0.7
Turbine inlet pressure (*bar*)	120

exiting the separator, and second, through Re1 and absorbing the excess heat of the vapor expanded in KC turbine. This basic solution enters the separator at point 10 after gaining sufficient energy from Re1 and Re2. Second, the temperature of the high-pressure condensed solution must be increased before entering SG. This happens in Re3 with the aid of the rich vapor that exits the separator. Again, in the thermally enhanced form of this cycle (EKC2), TEGs are integrated with the condensers to improve the power capacity of the whole cycle (Fig. 1 (d)).

3. Methodology

The energy, exergy, economic, and environmental analyses have been carried out on all four cycles, and results are elaborated by comparing their performance. Concurrently, an optimization problem will be solved to choose the best point with respect to the objective function and the constraints.

3.1. Initial assumptions

To ensure the physical possibility and comparability of cycle performances, some designing parameters are assumed to be constant during the analytical and optimization procedure. These assumptions are made using various authentic references in the literature and are listed in Table 5. For the simplicity of the modeling process, the

following assumptions are also considered:

- All components operate in steady-state conditions.
- Heat losses and pressure drops through the components and pipes are neglected.
- Variations of kinetic and potential energies are considered to be zero.

The whole cycle modeling and the optimization procedures are carried out employing MATLAB software integrated into the REFPROP 9 library as the reference for the thermodynamic properties of the fluids.

3.2. Energy and exergy modeling

For thermodynamic modeling, it is required to implement the mass and energy conservation laws, which are defined below [32,33]:

$$\sum \dot{m}_{in} = \sum \dot{m}_{out} \tag{1}$$

$$\dot{Q} + \sum \dot{m}_{in} h_{in} = \dot{W} + \sum \dot{m}_{out} h_{out} \tag{2}$$

Accordingly, the energy efficiency of each cycle can be calculated using Eq. (3):

$$\eta_{en} = \frac{\dot{W}_{net}}{\dot{Q}_{in}} \tag{3}$$

where, $\dot{Q}_{in}$ is equal to the thermal energy of the engine's exhaust gas and the produced power, $\dot{W}_{net}$ is equal to the summation of the generated power in the turbine and the consumed power in pumps (for the simple structures). However, for the enhanced configurations, the generated power in the thermoelectric generators is also added to the mentioned value.

$$\dot{Q}_{in} = \dot{H}_{HS1} - \dot{H}_{HS2} \tag{4}$$

$$\dot{W}_{net,SKC} = \dot{W}_{Tu} - \dot{W}_{Pu1} - \dot{W}_{Pu2} \tag{5}$$

$$\dot{W}_{net,EKC} = \dot{W}_{Tu} + \dot{W}_{TEG1} + \dot{W}_{TEG2} - \dot{W}_{Pu1} - \dot{W}_{Pu2} \tag{6}$$

The combination of the first and the second laws of thermodynamics results in the exergy balance equation as below [34]:

$$\dot{E}_Q + \sum \dot{m}_{in} e_{in} = \dot{E}_W + \sum \dot{m}_{out} e_{out} + \dot{E}_D \tag{7}$$

Table 6
The mass, energy, and exergy balance equations for system components.

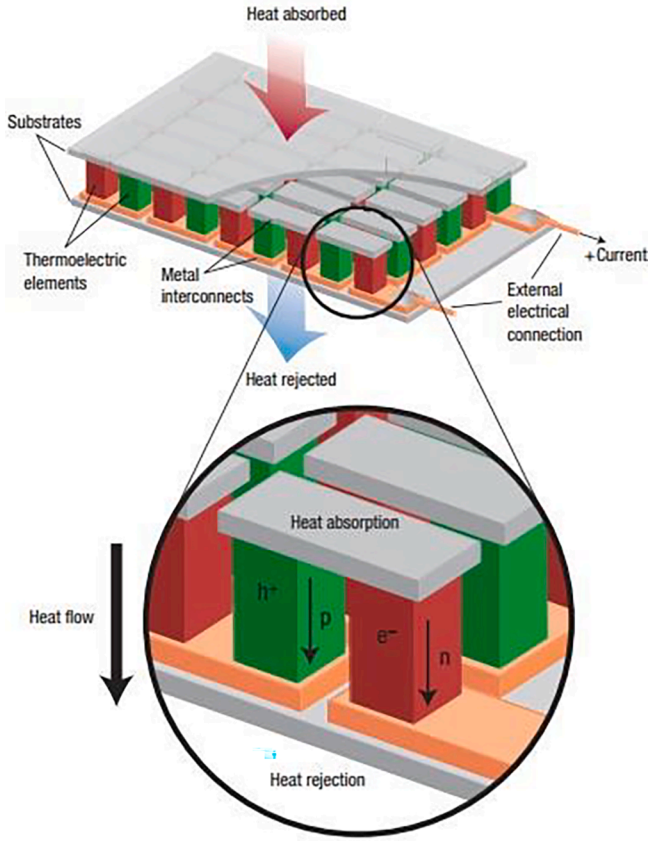| Component	Mass balance	Energy balance	Exergy balance
SKC1			
SG	$\dot{m}_{17} = \dot{m}_1, \dot{m}_{HS1} = \dot{m}_{HS2}$	$\dot{H}_{17} + \dot{H}_{HS1} = \dot{H}_1 + \dot{H}_{HS2}$	$\dot{E}_{17} + \dot{E}_{HS1} = \dot{E}_1 + \dot{E}_{HS2} + \dot{E}_D^{SG}$
Tu	$\dot{m}_1 = \dot{m}_2$	$\dot{H}_1 = \dot{H}_2 + \dot{W}_{Tu}$	$\dot{E}_1 + = \dot{E}_2 + \dot{W}_{Tu} + \dot{E}_D^{Tu}$
Re1	$\dot{m}_2 = \dot{m}_3, \dot{m}_{16} = \dot{m}_{17}$	$\dot{H}_2 + \dot{H}_{16} = \dot{H}_3 + \dot{H}_{17}$	$\dot{E}_2 + \dot{E}_{16} = \dot{E}_3 + \dot{E}_{17} + \dot{E}_D^{Re1}$
Re2	$\dot{m}_3 = \dot{m}_4, \dot{m}_9 = \dot{m}_{10}$	$\dot{H}_3 + \dot{H}_{13} = \dot{H}_{10} + \dot{H}_4$	$\dot{E}_3 + \dot{E}_{13} = \dot{E}_{10} + \dot{E}_4 + \dot{E}_D^{Re2}$
MX1	$\dot{m}_4 + \dot{m}_{13} = \dot{m}_5$	$\dot{H}_4 + \dot{H}_{13} = \dot{H}_5$	$\dot{E}_4 + \dot{E}_{13} = \dot{E}_5 + \dot{E}_D^{MX1}$
MX2	$\dot{m}_8 + \dot{m}_{11} = \dot{m}_{14}$	$\dot{H}_8 + \dot{H}_{11} = \dot{H}_{14}$	$\dot{E}_8 + \dot{E}_{11} = \dot{E}_{14} + \dot{E}_D^{MX2}$
CD1	$\dot{m}_5 = \dot{m}_6, \dot{m}_{CW1} = \dot{m}_{CW2}$	$\dot{H}_5 + \dot{H}_{CW1} = \dot{H}_6 + \dot{H}_{CW2}$	$\dot{E}_5 + \dot{E}_{CW1} = \dot{E}_6 + \dot{E}_{CW2} + \dot{E}_D^{CD1}$
CD2	$\dot{m}_{14} = \dot{m}_{15}, \dot{m}_{CW3} = \dot{m}_{CW4}$	$\dot{H}_{14} + \dot{H}_{CW3} = \dot{H}_{15} + \dot{H}_{CW4}$	$\dot{E}_{14} + \dot{E}_{CW3} = \dot{E}_{15} + \dot{E}_{CW4} + \dot{E}_D^{CD2}$
Pu1	$\dot{m}_6 = \dot{m}_7$	$\dot{H}_6 + \dot{W}_{Pu1} = \dot{H}_6$	$\dot{E}_6 + \dot{W}_{Pu1} = \dot{E}_7 + \dot{E}_D^{Pu1}$
Pu2	$\dot{m}_{15} = \dot{m}_{16}$	$\dot{H}_{15} + \dot{W}_{Pu2} = \dot{H}_{16}$	$\dot{E}_{15} + \dot{W}_{Pu2} = \dot{E}_{16} + \dot{E}_D^{Pu2}$
Sep	$\dot{m}_{10} = \dot{m}_{11} + \dot{m}_{12}$	$\dot{H}_{10} = \dot{H}_{11} + \dot{H}_{12}$	$\dot{E}_{10} = \dot{E}_{11} + \dot{E}_{12} + \dot{E}_D^{Sep}$
TV	$\dot{m}_{12} = \dot{m}_{13}$	$\dot{H}_{12} = \dot{H}_{13}$	$\dot{E}_{12} = \dot{E}_{13} + \dot{E}_D^{TV}$
Sp	$\dot{m}_7 = \dot{m}_8 + \dot{m}_9$	$\dot{H}_7 + \dot{H}_8 = \dot{H}_9$	$\dot{E}_7 + \dot{E}_8 = \dot{E}_9 + \dot{E}_D^{Sp}$
EKC1			
CD-TEG1	$\dot{m}_5 = \dot{m}_6, \dot{m}_{CW1} = \dot{m}_{CW2}$	$\dot{H}_5 + \dot{H}_{CW1} = \dot{H}_6 + \dot{H}_{CW2} + \dot{W}_{TEG1}$	$\dot{E}_5 + \dot{E}_{CW1} = \dot{E}_6 + \dot{E}_{CW2} + \dot{W}_{TEG1} + \dot{E}_D^{CD1}$
CD-TEG2	$\dot{m}_{14} = \dot{m}_{15}, \dot{m}_{CW3} = \dot{m}_{CW4}$	$\dot{H}_{14} + \dot{H}_{CW3} = \dot{H}_{15} + \dot{H}_{CW4} + \dot{W}_{TEG2}$	$\dot{E}_{14} + \dot{E}_{CW3} = \dot{E}_{15} + \dot{E}_{CW4} + \dot{W}_{TEG2} + \dot{E}_D^{CD2}$
SKC2			
Re3	$\dot{m}_{11} = \dot{m}_{15}, \dot{m}_{18} = \dot{m}_{19}$	$\dot{H}_{11} + \dot{H}_{18} = \dot{H}_{15} + \dot{H}_{19}$	$\dot{E}_{11} + \dot{E}_{18} = \dot{E}_{15} + \dot{E}_{19} + \dot{E}_D^{Re3}$

Fig. 2. Schematic visualization of a TE module showing the charge flow direction [36].
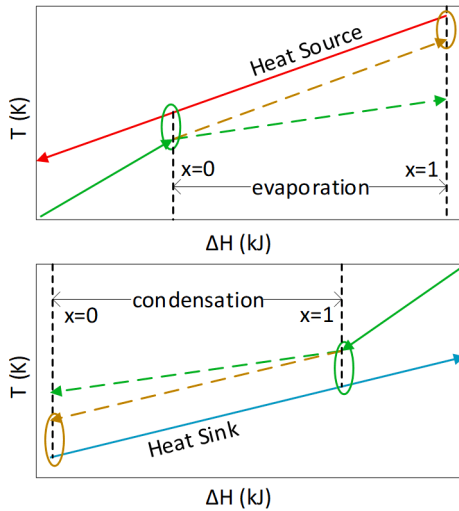

Fig. 3. The possible locations of pinch points in the phase change heat exchangers (evaporator and condenser).

in which, $\dot{E}_Q$, $\dot{E}_W$ denote the exergy rate of heat transfer and work output, respectively. $\dot{E}_D$ is the exergy destruction rate due to the irreversibilities of the system components. The specific flow exergy is defined as Eq. (8), considering the physical exergy and neglecting the chemical, potential, and kinetic exergies.

$$e = (h - h_0) - T_0(s - s_0) \tag{8}$$

As a result, the exergy efficiency of the whole cycle can be calculated

as below:

$$\eta_{ex} = \frac{\dot{E}_P}{\dot{E}_F} \tag{9}$$

For all Kalina cycles, the product exergy is the net output power, and the fuel exergy corresponds to the exergy rate provided by the exhaust gas of the Diesel engine, as described in Eqs. (10–12):

$$\dot{E}_F = \dot{E}_{HS1} - \dot{E}_{HS2} \tag{10}$$

$$\dot{E}_{P,SKC} = \dot{W}_{net,SKC} \tag{11}$$

$$\dot{E}_{P,EKC} = \dot{W}_{net,EKC} \tag{12}$$

The mass and energy conservation equations and the exergy balance equations of system components are listed in Table 6. These equations are used to calculate the values of generated or consumed power in turbine and pumps, respectively, as well as the input energy or exergy to the system.

3.2.1. TEG modeling

TEG modules are made of two dissimilar materials and can generate electricity via the Seebeck effect. The TE materials consist of tens to hundreds of TE couples connected electrically in series and thermally in parallel [35]. Seebeck effect makes TE materials produce voltage differences at the two ends of the unicouple under any change in the distribution of free charge carriers (electrons and holes) caused by the temperature gradient (Fig. 2) [23] (see Fig. 3.).

Assumptions mentioned below are considered to simplify the modeling equations of TEGs [23]:

- The thermal resistance between the TE module and heat source and heat sink is neglected.
- Heat transfer is one-dimensional and thermal losses are considered to be zero.
- The cross-sectional areas of the two branches are constant.
- The steady-state conditions are considered for flow modeling.
- The TE materials are embedded inside the condensers, in which the temperature gradient leads to produce the voltage difference.

As a heat engine, TEG absorbs thermal energy from the heat source and, while generating power from part of this energy, releases the remaining portion into the heat sink [35]:

$$\dot{Q}_h = \dot{Q}_c + \dot{W}_{TEG} \tag{13}$$

By expanding the equation above, Eq. (14) is developed. It is noteworthy that the equation describes the condensers' control volume in this study.

$$\dot{m}_h h_{h,in} - \dot{m}_h h_{h,out} = \dot{m}_c h_{c,out} - \dot{m}_c h_{c,in} + \dot{W}_{TEG} \tag{14}$$

Therefore, $\dot{W}_{TEG}$ can be calculated through the equation of TEG efficiency:

$$\eta_{TEG} = \frac{\dot{W}_{TEG}}{\dot{Q}_h} \tag{15}$$

On the other hand, TEG's efficiency solely depends on its material and hot and cold junctions' temperature [23]. Therefore, the value of η_{TEG} (as a characteristic of TEG) can be resulted by Eq. (16) [35]:

$$\eta_{TEG} = \eta_{Carnot} \frac{\sqrt{1 + ZT_m} - 1}{\sqrt{1 + ZT_m} + \frac{T_c}{T_h}} = \frac{\Delta T}{T_h} \frac{\sqrt{1 + ZT_m} - 1}{\sqrt{1 + ZT_m} + \frac{T_c}{T_h}} \tag{16}$$

where η_{Carnot} is the efficiency of Carnot heat engine working between the mentioned heat source and heat sink, T_c and T_h stand for the temperature of the heat sink and the temperature of the heat source, which can be defined as the average temperature of cold and hot streams in the

heat exchanger, respectively. T_m is the mean temperature of T_c and T_h:

$$T_m = \frac{T_c + T_h}{2} \tag{17}$$

Z is called the figure of merit of TEG material, which represents the internal conversion efficiency of TEG. This parameter is defined in $[\frac{1}{K}]$ and is directly related to the Seebeck coefficient, thermal conductivity, and electrical resistance of the material. Thus, in order to improve the efficiency of TEG, the value of Z should be enhanced. Since the mean temperature (T_m) also influence the TEG's efficiency, the dimensionless parameter of ZT_m is introduced as the dimensionless figure of merit, and its improvement is being investigated by scientists.

Currently, conventional materials have a ZT_m around 1 or less. Scientists have reported many materials with $ZT_m > 1.5$; however, few of them have been confirmed by other academic and industrial references [36]. For applications in the temperature range of 300–600 K, ZT_m can be considered to be 1 [37]. The average value of ZT_m varies from 0.5 to 0.9 [35]. All in all, in present work: $ZT_m = 0.9$.

3.2.2. Pinch point temperature difference

The phase change process of the ammonia-water mixture occurs in a non-isothermal process. Hence, the slope of temperature difference during these processes depends on the components (evaporator or condenser) and the composition of the zeotropic mixture. Consequently, the minimum temperature difference of the phase change processes can take place at either the beginning or the end of the process (Fig. 2). In order to locate the pinch point, the temperature difference between two hot and cold streams must be calculated throughout the phase change process. These calculations are performed concurrently with the modeling of the heat exchangers.

3.2.3. Optimization procedure

The optimization procedure is modeled in MATLAB and is dealt with by the *fmincon* solver. This solver is suitable for nonlinear, constrained problems. The first point in using this solver is to have two different MATLAB functions ready: the first one calculates the objective functions, and the second one includes the nonlinear constraints. Moreover, it requires the lower and upper boundaries of the decision variables, initial guess, solving algorithm, and the stopping criteria to run properly. The *fmincon* features several algorithms to solve different optimization problems. Here, SQP (Sequential Quadratic Programming) was selected since it showed a faster response than other algorithms within the given range of the decision variables. More explanations about this algorithm is presented in the Appendix. After triggering the process, the solver tries to locate a reasonable point within the vicinity of the initial guess. The objective and constraints functions run consecutively in each iteration to maximize/minimize the objective function while checking that no constraint is violated. The main criteria in selecting lower and upper boundaries for decision variables is that the selected values should guarantee appropriate answers without dealing with a huge range of numbers, thus, not taking it too long to find the optimum point. The upper and lower boundaries are first selected based on the initial assumptions of the system and also the ranges provided in similar research papers. Next, with trial and error, the ranges are modified in a way that they yield correct results without consuming so much time.

According to Zhang et al. [38], the properties of the turbine inlet stream, the turbine outlet pressure, and the separator inlet temperature play a significant role in the Kalina cycle performance. Here, similar to the procedure described in [20], the temperature, pressure, and mass fraction at the turbine inlet are fixed. Thus, the turbine outlet pressure and separator inlet temperature are selected as the decision variables to be found through an optimization procedure. However, the nature of the presented structures, just like many other complicated thermodynamic cycles, requires trial and error to find properties of some specific states (in this case, x_{10}, P_{15}, and T_{HS2}). Also, similar to any other optimization problem, there are one or several decision variables that are to be found

Table 7
The decision variables and the constraints of the optimization process with $\dot{W}_{net}$ as the objective function.

Cycle	Decision variables and their boundaries	Constraints
SKC1	$z_1 = P_2$: [400,800]	$\Delta T_{pp}^{HX} \geq \Delta T_{min}^{HX}$
	$z_2 = T_{10}$: [280,370]	$Q_2 \geq 0.9$
	$z_3 = x_{10}$: [0.5,0.7]	$0 \leq Q_{10} \leq 1$
	$z_4 = P_{15}$: [600,1200]	
	$z_5 = T_{HS2}$: [393,453]	
SKC2	$z_1 = P_2$: [200,800]	$\Delta T_{pp}^{HX} \geq \Delta T_{min}^{HX}$
	$z_2 = T_{10}$: [280,370]	$Q_2 \geq 0.9$
	$z_3 = x_{10}$: [0.5,0.7]	$0 \leq Q_{10} \leq 1$
	$z_4 = P_{17}$: [600,1200]	
	$z_5 = T_{HS2}$: [393,453]	

in an iterative manner (P_2 and T_{10} in this study, as just mentioned above). Here, as an approach to conduct the optimization faster, all the parameters that are needed to be found iteratively are considered as the decision variables in for the objective function. Moreover, to pinpoint the exact location of the pinch point in the second condenser, its pressure must also be found in an iterative way. To find these parameters in a conventional manner, loops can be used in the simulations. Nevertheless, in the current research, to make the calculations faster and avoid burdensome iterations, the mentioned parameters are also considered as the decision variables in the optimization problem.

This optimization maximizes the net power generated by each cycle with the given initial conditions. Here, the pinch point violation is the most highlighted constraint, which is calculated using the method that is already discussed. Also, the stack dew point temperature and stream quality at the turbine outlet and the separator inlet must meet feasible conditions. The lower and upper bounds of the decision variables are chosen in a way to prevent the critical points while they guarantee to find the optimum global point. Table 7 shows the details of the decision variables and constraints for SKC1 and SKC2.

For a graphical illustration, the developed algorithm for the SKC1 is explained in a flow chart depicted in Fig. 4. This algorithm is repeated until it reaches the global maximum of the objective function.

3.3. Economic analysis

Conducting the economic analysis of the cycles' performances will provide useful results that present the factors responsible for the cycle's economic drawbacks and positive points, thereby recognizing the economic characteristics of the cycles that should gain more attention in system design and optimization. Furthermore, regardless of the positive and negative achievements of thermal evaluation, the economic analysis helps researchers assess the feasibility or profitability of embedding TEGs in the condensers of high-temperature Kalina cycles.

The thermo-economic tools can be employed as the first step in economic study. Thermoeconomics (i.e., exergoeconomics) combines exergy analysis and economic principles to provide essential information, the most substantial of which are as follow [39,40]:

- To diagnose the cost sources regarding the thermodynamic (i.e., exergetic) deficiencies.
- To determine the production cost rates of each product in the energy conversion systems with various products.
- To understand the cost-formation process and the flow of costs in an energy conversion system.
- To facilitate the optimization and process improvement studies relying on the economic losses attributed to the system components.

The Specific Exergy Costing (SPECO) approach is the most popular method of thermoeconomic assessment, which is used in this work to conduct the cost balance equations for the components of the cycles under study [41]. Two steps of the SPECO method (identifying the
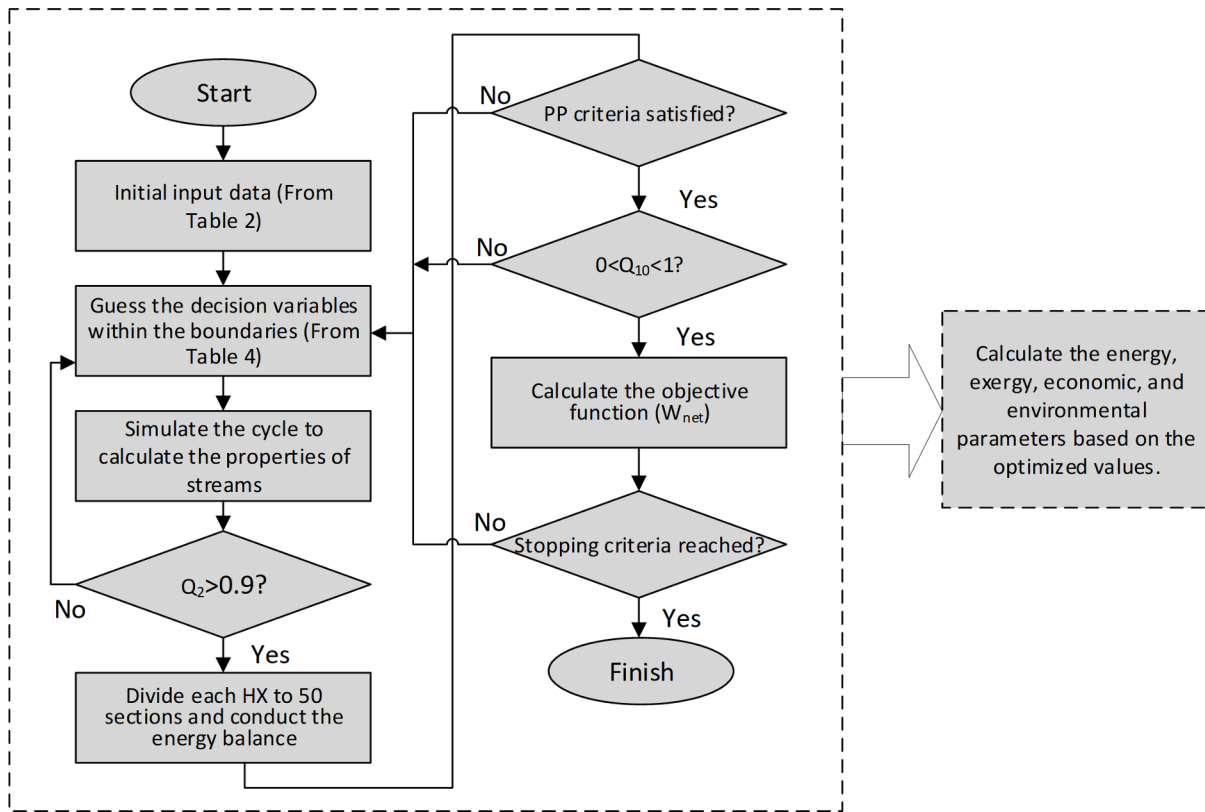
Fig. 4. The algorithm of the optimization process.

exergy of streams and defining the fuel and the product exergies in each component) were introduced thoroughly in previous sections. The last step (cost balance equations) is taken for system components by applying the equations below [42]:

$$\dot{C}_P = \dot{C}_F + \left(\dot{C}_{CI} + \dot{C}_{OM}\right)_k \tag{18}$$

$$\dot{C}_F = c_F \dot{E}_F \tag{19}$$

here, $\dot{C}_P$ corresponds to the product cost rate in (US\$/h), and $\dot{C}_F$ stands for the fuel cost rate that can be calculated using Eq. (19). When Eq. (18) is applied for the whole cycle, $\dot{C}_F$ represents the cost of the engine's exhaust gas.

In this condition, since in conventional Diesel engine-based power plants without the exhaust gases' waste heat recovery strategy, these gases are discharged into the environment, it is a rational assumption to consider that the engine's exhaust gases have no economic value ($c_F = \dot{C}_F = 0$) [21]. In addition, $\dot{C}_{CI}$ and $\dot{C}_{OM}$ represents the costs associated to the Capital Investment (CI) and Operation and Maintenance (OM), respectively.

$$\left(\dot{C}_{CI} + \dot{C}_{OM}\right)_k = \frac{(TI \times CRF \times \phi) + (FI \times CELF)}{365 \times 24 \times CF} \tag{20}$$

Here, CRF is the capital recovery factor that is defined to calculate the present value of equal annual cash flows as below [34,41]:

$$CRF = \frac{i(1+i)^{LT}}{(1+i)^{LT} - 1} \tag{21}$$

In the above equation, i is the interest (discount) rate, which is considered to be 0.08, and LT is the cycle's lifetime, regarded as 20 years. CF is 0.8, which defines as the capacity factor. CELF is the short form of the Constant Escalation Levelization Factor and applies the effect of the inflation rate on the operation and maintenance costs [43]:

Table 8
Description of various initial cost coefficients as a fraction of *PC* [10].

Cost coefficient	Description	Value (fraction of PC)
C_{Su}	Startup costs	0.05
C_{Eq}	Equipment installation costs	0.20
C_{St}	Structural costs	0.25
C_S	Service facilities	0.20
C_{Con}	Contingencies	0.06
C_{La}	Land cost	0.10

Table 9
PC functions of the system components [21,26,30,45–47].

Component	PC equation	Reference year	$CEPCI_{ref}$*
Pump	$PC_{Pu} = 1120\dot{W}_{Pu}^{0.8}$	2005	468.2
Turbine	$PC_T = 6000\dot{W}_T^{0.7}$	2012	584.6
TEG	$PC_{TEG} = PEC_{CD} + c_{TEG}\dot{W}_{TEG}$ $c_{TEG} = 2000\$/kW$	2019	607.5
Heat exchangers	$PC_{HX} = Y_1 \left(\frac{A_{HX}}{Y_2}\right)^{Y_3}$ $A_{HX} = \frac{\dot{Q}}{U\Delta T_{ln}}$	2008	575.5

* $CEPCI_{2020} = 596.2$[10].

$$CELF = \frac{k_{OM}\left(1 - k_{OM}^{LT}\right)}{1 - k_{OM}} CRF \tag{22}$$

$$k_{OM} = \frac{1+r}{1+i} \tag{23}$$

r is the inflation rate, which is considered to be 0.02. Operation and maintenance costs are usually considered as a percentage of the capital investment. Therefore, the annual escalation factor of operating and

Table 10

Coefficients of heat exchangers' cost equations [16,48,49].

Heat exchanger	$Y_1(\$)$	$Y_2(m^2)$	Y_3	$U(kW/m^2K)$
Steam generator	17,500	100	0.6	1.6
Recuperator	12,000	100	0.6	1
Condenser	8000	100	0.6	1.1

maintenance costs with the value of 0.06 is multiplied by *TI* [44].

In Eq. (20), *FI* and *TI* are fixed capital investment and total capital investment, respectively, and can be estimated using the equations below [34]:

$$TI_k = FI_k + C_{Su}PC_k \tag{24}$$

$$FI_k = \left(1 + C_{Eq} + C_{St} + C_S + C_{Con} + C_{La}\right)PC_k \tag{25}$$

PC_k denotes the purchase equipment cost of each component in (\$), which can be multiplied with the coefficients of inevitable costs in power plant establishment to result in *FI*. Meanwhile, *TI* is equal to *FI* plus startup costs, which can be estimated by multiplying a coefficient with *PC*. The value of all the coefficients corresponding to the additional investment costs is provided in Table 8 as the fraction of *PC*.

The *PC* equations of system components are described in Table 9. The investment costs of the flash separators and mixing chambers are neglected due to their relatively low values compared to the other components. For the thermoelectric generator, since it is a module that is appended to the condensers, it is rational to consider its capital investment cost equal to the condenser cost plus the module cost [30]. The cost associated with the heat exchangers depends on the area of the heat transfer surface (A_{HX}) and the phase of fluids participating in the heat exchange process.

Y_1, Y_2, and Y_3 coefficients are described in Table 10 for steam generator, condenser, and recuperator.

The total capital investment and operation and maintenance costs of cycles can be deduced by the summation of those components. As a result, after calculating the product cost of the cycles, the Levelized Cost of Electricity (LC) in $/GJ$ can be calculated through Eq. (26) for each cycle:

$$LC = \frac{\dot{C}_P}{\dot{W}_{net}} \tag{26}$$

Some essential economic indicators include but are not limited to the net present value, annual profit, and discounted payback period. These indices estimate a plant's net profit considering the cost of electricity produced to be sold to the grid [10]. Net present value (PV) estimates the present value of achieved profit, which is the summation of all cash inflows and outflows during the lifetime of the plant, and can be calculated through the equation below [10]:

$$PV = -TI + \sum_{t=1}^{LT} \frac{AP \times (1+r)^{t-1}}{(1+i)^t} \tag{27}$$

Annual profit (AP) can be calculated by subtracting the yearly OM costs from the annual profit from the power sale [10,50]:

$$AP = \left(\dot{W}_{net} \times 365 \times 24 \times CF \times C_{Se} - FI \times CELF \times \phi\right) \times (1-\tau) \tag{28}$$

in which, C_{Se} denotes the unit price of electricity sold to the grid, which is considered to be 0.1 $/kWh$ [51], and τ stands for the tax rate, which equals 25 % [50].

The discounted payback period (PP) is another economic indicator that equals the amount of time needed to recover the capital investment of a project completely, which in other words, is the time needed for the PV to become zero [10]:

Table 11

Validation of Kalina cycles based on the results of Ref. [20].

Study	$P_2(bar)$	x_{10}	$T_{17}(°C)$	$\eta(\%)$
Modi and Haglind [20]	6.04	0.6795	134.2	31.46
This study	6.05	0.6780	134.3	31.39
Relative difference (%)	0.17	−0.22	0.07	−0.22

Table 12

Comparing the results of TEG modeling in the present work with those in Ref. [26] ($ZT_m = 1$).

Study	$\dot{Q}_c(kW)$	$\dot{W}_{TEG}(kW)$	$\eta_{TEG}(\%)$	$Ex^D_{TEG}(kWh)$
Nabat et al. [26]	1525.472	13.82	0.905	246.6
This study	1526	13.93	0.905	248.1
Relative difference (%)	0.03	0.80	0.00	0.61

$$PP = \frac{\ln\left(\frac{TCI \times (r-i)}{AP} + 1\right)}{\ln\left(\frac{1+r}{1+i}\right)} \tag{29}$$

3.4. Environmental analysis

In addition to thermodynamic and economic assessment of the systems, environmental issues are highly important today. Hence, environmental assessments are also necessary for systems that provide a way to reduce emissions of air pollutants and conserve fuels.

According to Ref. [52], decreased carbon dioxide emission in a system that works based on waste heat recovery is equal to the carbon dioxide that would have been emitted if the generated power from waste heat recovery was to be produced by the gas turbine or Diesel engine. Based on mass analysis of the exhaust gas, the considered Diesel engine produces 0.051 kg/s carbon dioxide when it delivers 320 kW of power. Hence it can be concluded that to produce 1 kWh of energy using this engine, 0.58 kg of carbon dioxide will be released into the atmosphere. Moreover, the required fuel in this Diesel engine is calculated as 0.26 L/kWh (According to Table 1 and simple calculations). Finally, the values of avoided carbon dioxide and saved fuel is calculated using Eqs. (30) and (31), respectively [53].

$$CO_{2,AV} = 0.58 \times \dot{W}_{net,KC} \tag{30}$$

$$fuel_{SV} = 0.26 \dot{W}_{net,KC} \tag{31}$$

4. Results

The results of 4E analyses conducted on four proposed WHR cycles are elaborated in this section. In order to make it effortless to study, the results and related discussions are provided in separate sections.

4.1. Validation

To ensure that the results are authentic and accurate enough, first, it is tried to compare the results with a similar study. In this regard, the study conducted by Modi and Haglind [20] is selected, which has considered four different structures of optimized high-temperature

Table 13

The values of decision variables at the optimum points of SKC1 and SKC2.

Decision variable	SKC1	SKC2
$z_1 = P_2(kPa)$	455.68	296.65
$z_2 = T_{10}(K)$	361.94	356.09
$z_3 = x_{10}$	0.55	0.46
$z_4 = P_{15}(kPa)$	694.94	695.67
$z_5 = T_{HS2}(K)$	419.76	393.15

Table 14
The comparison between the optimization methods and their calculation times in the present work, Marston [19], and Modi and Haglind [20].

Study	Utilized method	Pinch point constraint	Required time
Marston [19]	Trial and error	No	11 h
Modi and Haglind [20]	GA (MATLAB)	Yes	50 min
This study	fmincon (MATLAB)	Yes	5–8 min

Kalina cycles. Table 11 shows a comparison between the results of the procedure used in the current study and the results obtained from Ref. [20]. The procedure to generate the results of the validation is exactly the same as what is explained in Section 3. However, structures and initial assumptions are exactly chosen according to the reference papers and are implemented in the developed MATLAB code. The results of this validation indicate the developed code for this study is accurate and the results that presented in the rest of this section are reliable.

The energy and exergy modeling of TEG is validated based on the results of Nabat et al. [26], and the comparisons are presented in Table 12:
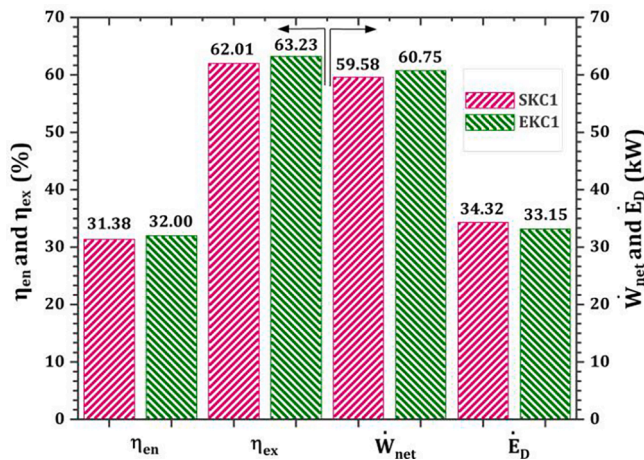
Table 15
The values of thermodynamic variables for SKC1 (and EKC1).

Stream	$\dot{m}(kg/s)$	x	T(°C)	P(bar)	h(kJ/kg)	s(kJ/kgK)	e(kJ/kg)
1	0.08	0.70	514.20	120	3008.8	7.17	15,139
2	0.08	0.70	181.23	4.56	2266.8	7.48	14,307
3	0.08	0.70	100.32	4.56	1739.3	6.13	13,871
4	0.08	0.70	44.76	4.56	874.34	3.65	14,036
5	0.13	0.55	60.13	4.56	655.96	2.88	10,981
6	0.13	0.55	27.00	4.56	52.98	0.96	10,940
7	0.13	0.55	27.05	6.95	53.39	0.96	10,941
8	0.05	0.55	27.05	6.95	53.39	0.96	10,941
9	0.08	0.55	27.05	6.95	53.39	0.96	10,941
10	0.08	0.55	88.79	6.95	918.39	3.56	11,043
11	0.03	0.93	88.79	6.95	1861.47	6.61	18,775
12	0.05	0.29	88.79	6.95	292.70	1.54	5910
13	0.05	0.29	78.22	4.56	292.70	1.54	5909
14	0.08	0.70	47.51	6.95	774.53	3.25	14,054
15	0.08	0.70	27.05	6.95	166.65	1.28	14,025
16	0.08	0.70	29.70	120	188.38	1.30	14,041
17	0.08	0.70	131.27	120	715.88	2.80	14,129
HS1	0.45	–	529.20	1.01	971.30	7.63	239.66
HS2	0.45	–	146.61	1.01	546.58	6.91	24.72
CW1	1.91[a]	–	20.00	1.01	84.01	0.30	0.00
CW2	1.91[b]	–	30.00	1.01	125.82	0.44	0.70
CW3	1.20[c]	–	20.00	1.01	84.01	0.30	0.00
CW4	1.20[d]	–	30.00	1.01	125.82	0.44	0.70

For EKC1 (a = 1.89, b = 1.89, c = 1.18, and d = 1.18 kg/s).

Table 16
The values of thermodynamic variables for SKC2 (and EKC2).

Stream	$\dot{m}(kg/s)$	x	T(°C)	P(bar)	h(kJ/kg)	s(kJ/kgK)	e(kJ/kg)
1	0.08	0.70	514.20	120	3008.8	7.17	15,139
2	0.08	0.70	150.42	2.97	2202.1	7.54	14,226
3	0.08	0.70	66.15	2.97	1248.1	4.90	14,043
4	0.21	0.46	54.49	2.97	476.51	2.30	9152
5	0.21	0.46	27.00	2.97	9.25	0.81	9123
6	0.21	0.46	27.07	6.96	9.91	0.81	9123
7	0.04	0.46	27.07	6.96	9.91	0.81	9123
8	0.17	0.46	27.07	6.96	9.91	0.81	9123
9	0.17	0.46	56.15	6.96	185.21	1.36	9136
10	0.17	0.46	82.94	6.96	607.57	2.59	9196
11	0.04	0.95	82.94	6.96	1833.67	6.55	19,129
12	0.13	0.32	82.94	6.96	263.58	1.48	6409
13	0.13	0.32	37.07	6.96	39.10	0.81	6382
14	0.13	0.32	37.13	2.97	39.10	0.81	6382
15	0.04	0.95	39.73	6.96	1515.54	5.61	19,089
16	0.08	0.70	46.29	6.96	755.02	3.19	14,053
17	0.08	0.70	27.08	6.96	166.83	1.28	14,025
18	0.08	0.70	29.73	120	188.56	1.30	14,041
19	0.08	0.70	60.80	120	345.99	1.79	14,053
HS1	0.45	–	529.20	1.01	971.30	7.63	239.66
HS2	0.45	–	120.00	1.01	518.41	6.84	16.88
CW1	2.35[a]	–	20.00	1.01	84.01	0.30	0.00
CW2	2.35[b]	–	30.00	1.01	125.82	0.44	0.70
CW3	1.07[c]	–	20.00	1.01	84.01	0.30	0.00
CW4	1.07[d]	–	30.00	1.01	125.82	0.44	0.70

For EKC2 (a = 2.33, b = 2.33, c = 1.05, and d = 1.05 kg/s).

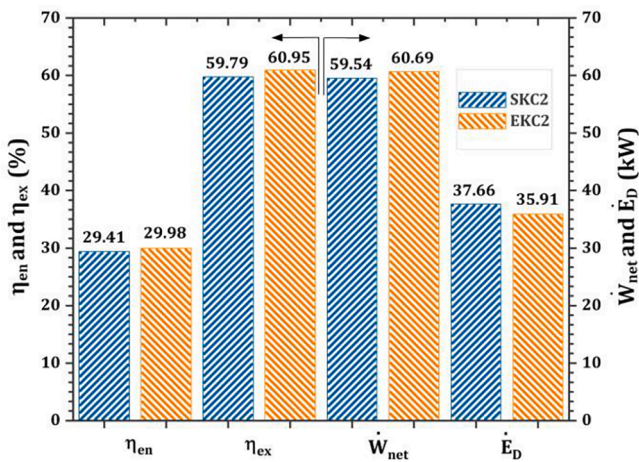**Fig. 5.** Comparison between the performance criteria of SKC1 and EKC1.

Fig. 6. Comparison between the performance criteria of SKC2 and EKC2.

4.2. Optimization results

The optimization procedure is carried out to maximize the net output power produced by each KC under the variation range of decision variables. The values of points on which the decision variables give the maximum net power are listed for SKC1 and SKC2 in Table 13. The optimum value for all the variables is within the defined range for the optimization problem.

As mentioned earlier, one of the main objectives of this study was to find an alternative solution to obtain the desired results in a faster way. Initially, Marston [19] decided to find the ammonia mass fraction at the separator inlet by the trial and error method. After each iteration, the guessed value was compared with the new value that was found by the cycle simulation. This continued until the error between the two values was negligible.

The mentioned procedure took more than 11 h. Later, Modi and Haglind [20] decided to choose the above-mentioned parameter as an optimization decision variable in order to reduce the calculation time. They used the Genetic Algorithm (GA) method to conduct their research. According to their approach, the calculations could be finished in a much shorter time, almost 50 min. Notably, their method included dividing each heat exchanger into 50 sections to check the pinch point, which made the calculations more complicated; yet the calculation time was much shorter compared to the previous ones.

In the current study, as mentioned before, *fmincon* solver is chosen to carry out the optimization process. To make a step forward, it is seen

Table 17
The performances of TEG modules used in EKCs.

Component	$\dot{W}_{TEG}(kW)$	$\eta_{TEG}(\%)$
TEG1 in EKC1	0.82	1.03
TEG2 in EKC1	0.35	0.69
TEG1 in EKC2	0.86	0.88
TEG2 in EKC2	0.29	0.66

that the optimization process with the selected method requires significantly less time, which is within the range of 5 to 8 min. This reduces the required time by the previous study by about 90 %. Table 14 summarizes the explanations stated above with relevant references.

4.3. Energetic and exergetic performance of Kalina cycles

The values associated with the thermodynamic parameters are presented in Tables 15 & 16, respectively, for the optimum points of SKC1 (and EKC1) and SKC2 (and EKC2). By employing TEGs in the condensers, the mass flow rates of cooling waters tend to flow down slightly.

As evident in Figs. 5 and 6, both charts subscribe to the positive effects of TEG embedding on the performance criteria of Kalina cycles. TEGs improve the efficiencies of SKC1 and SKC2 while reducing their exergy destruction rates. However, both Figs. 5 and 6 show that the magnitude of enhancement in the power output and the efficiencies of Kalina cycles is not considerable.

The mitigation of exergy destruction rates of EKC1 and EKC2 is due to the decrement of the value of this parameter as a result of useful exergy production (power) carried out by TEG modules. The enhancements provided by TEG modules are presented in Table 17. Furthermore, comparing the performance indices of SKC1 and SKC2, it is deduced that SKC1 and, thereby, EKC1 demonstrate more desirable performance than SKC2 and EKC2, respectively. The privilege of SKC1 (and EKC1) over SKC2 (and EKC2) is noticeable in terms of efficiencies and exergy destruction rate. The difference between their power outputs is not considerable.

The exergy destruction rates of system components of SKC1 are illustrated in Fig. 7. It is shown in Fig. 7 that the highest amount of exergy destruction rate is attributed to the steam generator and turbine, respectively. Phase changing and large temperature differences between fuel and product exergy flows in these devices are the main reasons for the high exergy destruction rate. Embedding TEG modules in condensers improves their exergetic performances by reducing the exergy destruction rates of Cd1 and Cd2, respectively, from 4.03 and 1.55 kW in SKC1 to 3.21 and 1.21 kW in EKC1. The same happens in the SKC2, for Cd1 and Cd2, respectively, from 4.54 and 1.33 kW (Fig. 8) to 3.68 and 1.04 kW in EKC2.

According to Figs. 7 and 8, the exergy destruction rate of the steam generator in SKC2 is considerably higher than that of SKC1. The working fluid entering SG in SKC1 (stream 17) has a higher temperature, resulting in a lower exergy difference with the exhaust gases.

On the other hand, the exergy difference between the working fluid entering SG in SKC2 (stream 19) and the exhaust gases is higher due to the lower temperature of stream 19 compared with that of exhaust gas. These differences cause a considerable difference in destructed exergies within the steam generators of SKC1 and SKC2. The results of Figs. 7 and 8 also acknowledge the advantages of SKC1 and EKC1 over SKC2 and EKC2, respectively.

4.4. Economic and environmental performance of Kalina cycles

It was expected that the enhanced forms of Kalina cycles would have higher total capital investment costs than the simple ones, which is also revealed in Fig. 9. As a result, the levelized cost of produced electricity of enhanced KCs will be higher than that of simple cycles. Moreover, the thermodynamical privilege of EKCs over the SKCs, due to the application
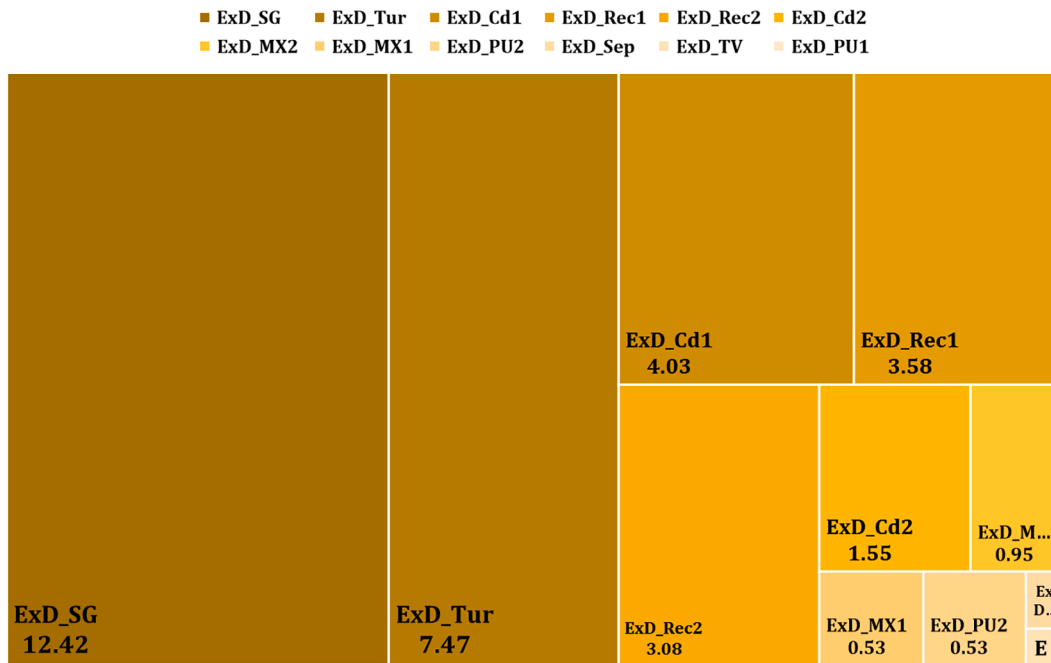
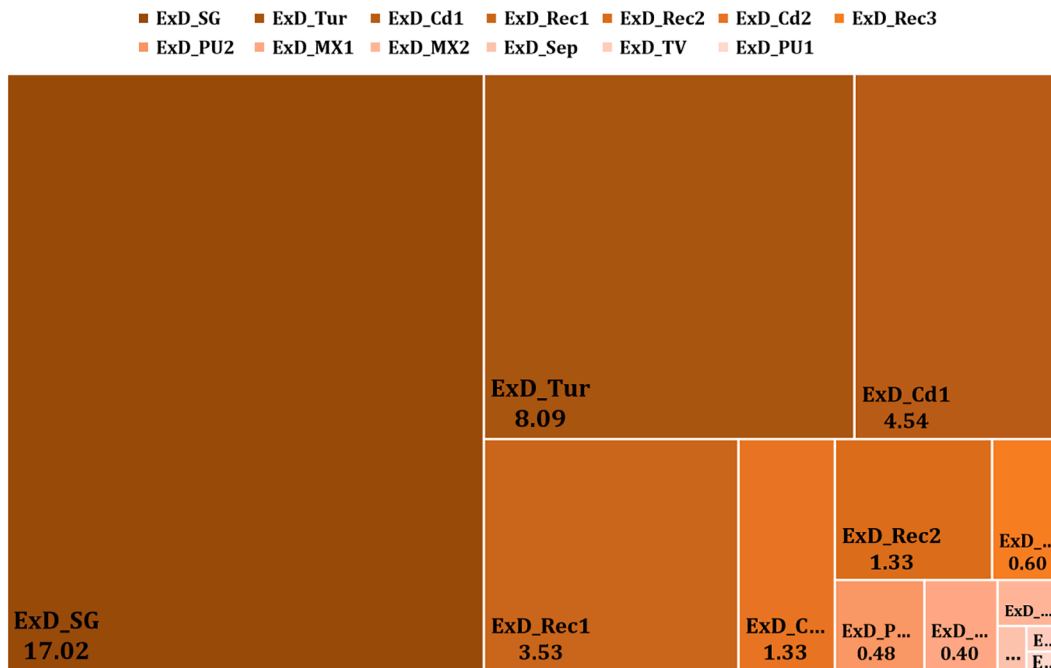**Fig. 7.** Exergy destruction rates of SKC1′s components (*kW*).

Fig. 8. Exergy destruction rates of SKC2′s components (kW).

of TEGs, results in a higher net present value and payback period for EKCs. Nevertheless, the differences are too small and thus negligible. According to Fig. 10, the net present values of SKC2 and EKC2 are higher than those of SKC1 and EKC1, respectively. This difference is relatively considerable, which is 86.63 *k*$ for SKC2, while it is 84.56 *k*$ for SKC1.

The efficient components of KC1 demand higher investment and OM costs; therefore, KC2 is a cost-effective system compared with KC1. Furthermore, Fig. 10 exposes that the more the PV is, the less the payback period is expected to be. This is also deducible from the definition of PV according to Eq. (27). PV is the accumulative profit of each cycle during its lifetime, so the higher profits make it earlier to

compensate for the costs of each cycle.

Regarding Eqs. (30) & (31), the more power is produced, the more carbon dioxide would be avoided, and thus, the more fossil fuel would be saved. This is why the enhanced KCs have desirable performances from the environmental perspective, as shown in Fig. 11. Another notable result exposed in Fig. 11 is that the amount of avoided CO_2 and saved fossil fuel for both SKC1 (or EKC1) and SKC2 (or EKC2) are relatively same since their power outputs are almost equal.
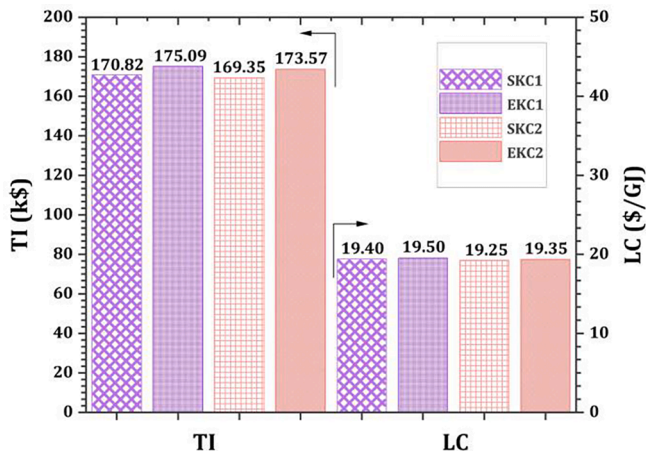
Fig. 9. Comparison between TI and LC of four KCs.
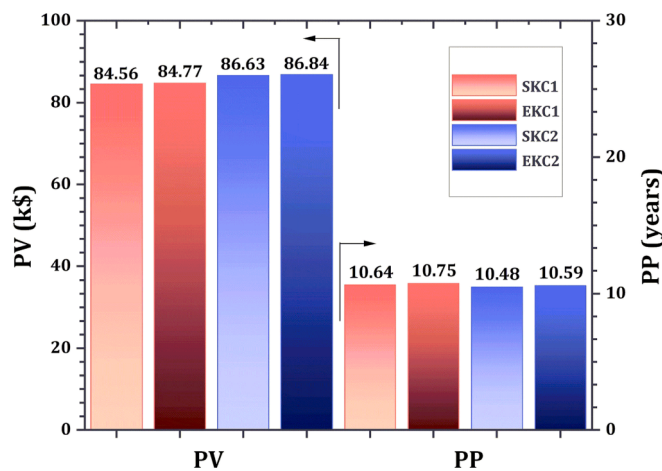
Fig. 10. Comparison between PV and PP of four KCs.
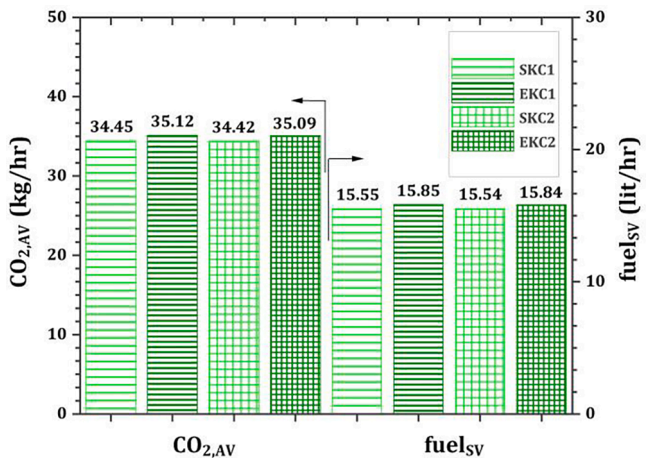
Fig. 11. Comparison between the environmental indices of four KCs.

4.5. Parametric study

A parametric study is conducted to study the behavior of performance criteria of four Kalina cycles under the variations of variables. All results are presented for the optimum performance of cycles. However, to avoid redundant content, among the similar performance criteria, one
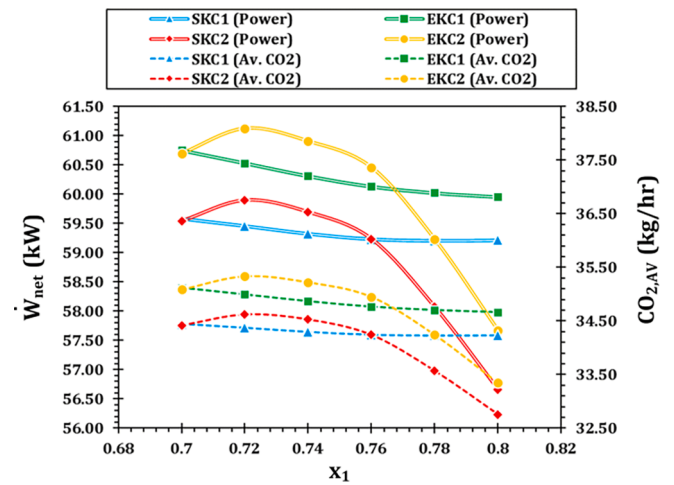

Fig. 12. Variation of net power output and avoided CO_2 with the variation of x_1.
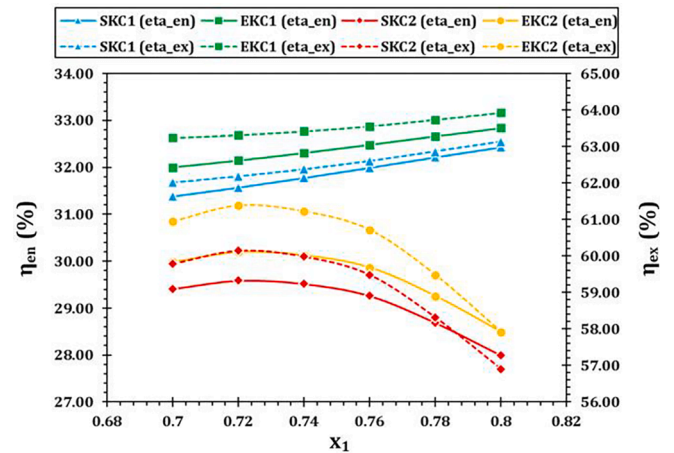
Fig. 13. Variation of energy and exergy efficiencies with the variation of x_1.

of them has been considered to be studied in this section.

4.5.1. The effect of the variation of ammonia mass fraction at the turbine inlet

Fig. 12 demonstrates the net power behavior and avoided CO_2 diagrams as the results of variations of ammonia mass fraction at the turbine inlet. It is shown that the net power output, and thus, the avoided CO_2 tend to decrease with increasing the ammonia mass fraction. To justify their behaviors, more elaboration is made. First, it should be noted that the SKC1 does not require using all the available energy from the heat source due to sufficient recuperation. In other words, it does not cool the exhaust gas stream until its dew point limit.

Adversely, because of less efficient recuperation in SKC2, all the provided heat by the exhaust gas is used in this system. Thus, the input energy of the SKC1 and EKC1 may vary with different assumptions, while the SKC2 and EKC2 are proved to have constant input energy, no matter what the assumptions are. For the SKC1 and EKC1, with the increase of x_1, the input energy from the heat source and dissipated energy through the condensers tend to decrease. However, the decrease rate of the input heat is slightly more than that of the dissipated heat. Thus, according to the first law of thermodynamics, the total net power will decline with a smooth steep as x_1 rises. For the SKC2 and EKC2, a fluctuation is seen in their behavior against changing x_1. As stated above, the input energy remains constant. Hence, the behavior of the net generated power will depend solely on the behavior of the dissipated
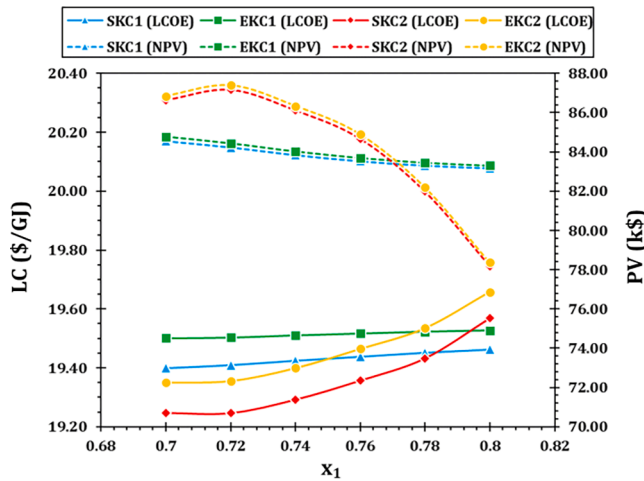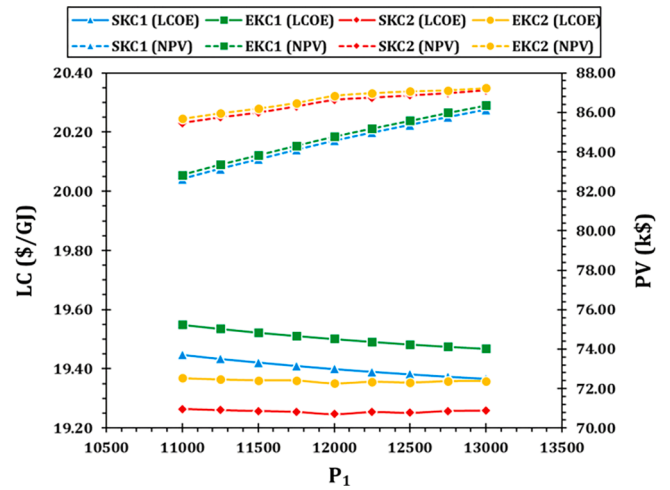
Fig. 14. Variation of LC and PV with the variation of x_1.
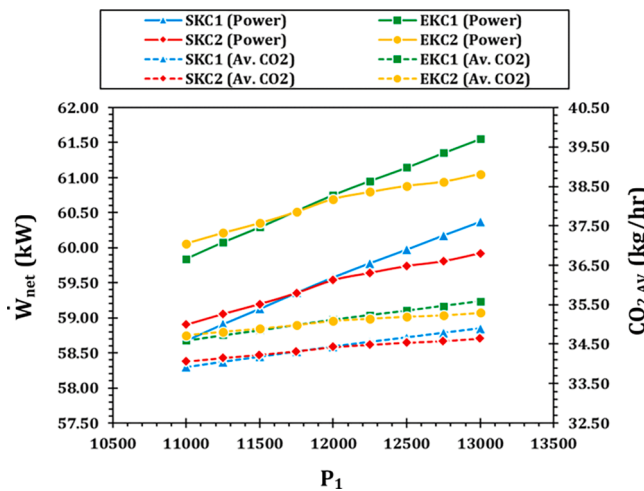

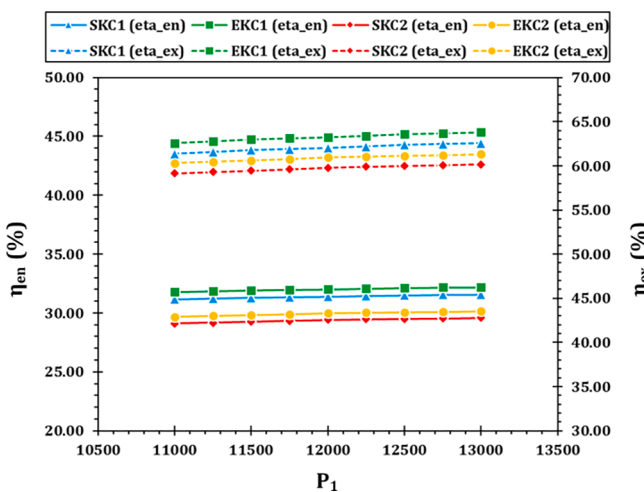Fig. 15. Variation of net power output and avoided CO_2 with the variation of P_1.

Fig. 16. Variation of energy and exergy efficiencies with the variation of P_1.

Fig. 17. Variation of LC and PV with the variation of P_1.

change of x_1. This is simply due to the fact that the denominator of the efficiency equation (input heat) tends to decrease at a faster pace than the numerator of the efficiency equation (generated power). Thus, the efficiency increases. For the KC2 cycles, since the input energy remains the same, the efficiencies behave the same as the generated power.

It can be concluded that for ammonia mass fractions from 0.7 to 0.76, the best choice in terms of power output is SKC2, compared to SKC1. This range is 0.704 to 0.768 for the privilege of EKC2 over EKC1. Nevertheless, Fig. 13 shows that both types of KC1 are superior to KC2 in terms of energy and exergy efficiencies. Ultimately, the ammonia mass fraction of 0.8 leads to the maximum energy efficiency of 32.84 % and exergy efficiency of 63.92 % for the EKC1 case.

The reduction in the net power output of all Kalina cycles with increasing the ammonia mass fraction results in a slight growth in the value of the levelized cost of electricity (Fig. 14). This rise is more tangible for KC2 owing to the sharp reduction occurs in its power production with mass fraction increasing compared to KC1.

Consequently, the net present value of Kalina cycles presents a counter behavior in Fig. 14. Because the more cost associated with the electricity production, the less profit accumulated during the years. The variations of PVs of the KC1 cycles are within the 84.77–83.17 k\$ range, while this range is 86.84–78.17 k\$ for the KC2 cycles under the variation of ammonia mass fraction (x_1) from 0.7 to 0.8.

4.5.2. The effect of the variation of turbine inlet pressure

It is obvious that the more pressure at the turbine inlet, the more power will be generated. The increasing trend for the net power output, the avoided CO2, and the energy and exergy efficiencies are obvious in Figs. 15 & 16, respectively.

Increasing the turbine inlet pressure causes an increase in the outlet temperature of the turbine while indirectly increasing the mass flow rate of working fluids in Kalina cycles. While the change in the possibly effective parameters can be neglected, the mass flow rate of the working fluid in KC1 increases by about 0.8 %, whereas this value is 0.3 % for KC2. Therefore the slope of variation of the net power output of KC1 cycles in Fig. 15 is more than that of KC2 cycles. The same trend is also seen for energy and exergy efficiencies in Fig. 16.

Without any doubt, any increase in the turbine inlet pressure will cause an increase in both the net power output and the investment cost of the turbine. However, the improvement of net power output is more distinguished from the increment of the investment costs of the turbine. Accordingly, the LC of four KCs tends to decrease slightly with the increase of P_1, as presented in Fig. 17. The secondary effect of diminishing the LC is increasing the accumulative profit of selling the electricity, which is defined by the positive trend of PV in Fig. 17.
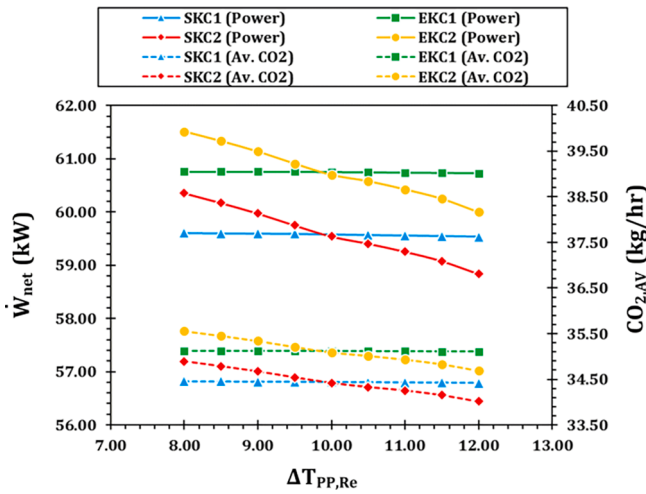
heat through the condensers, so it is more vulnerable to fluctuations and sudden changes.

As seen in Fig. 13, although the net generated power of KC1 cycles tends to decline, their energy and exergy efficiencies rise with the

Fig. 18. Variation of net power output and avoided CO₂ with the variation of..ΔT_{pp}^{Re}
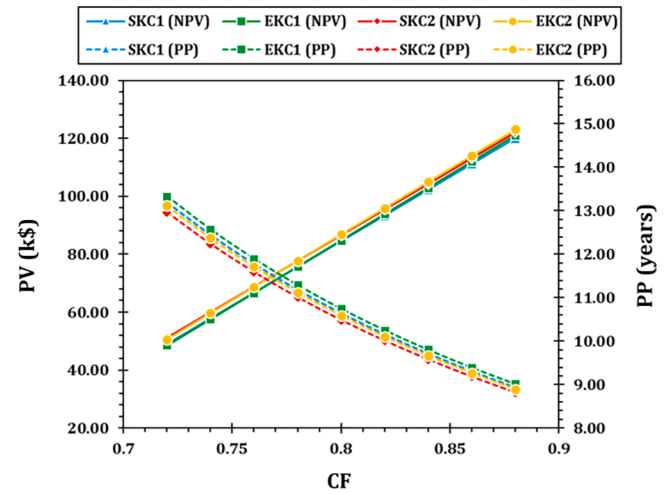
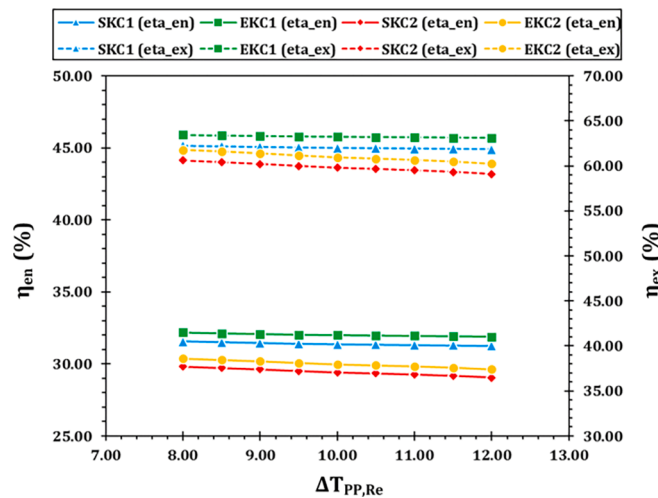**Fig. 19.** Variation of energy and exergy efficiencies with the variation of..ΔT_{pp}^{Re}

Fig. 20. Variation of LC and PV with the variation of..ΔT_{pp}^{Re}

Fig. 21. Variation of PV and PP with the variation of the cycles' capacity factor.
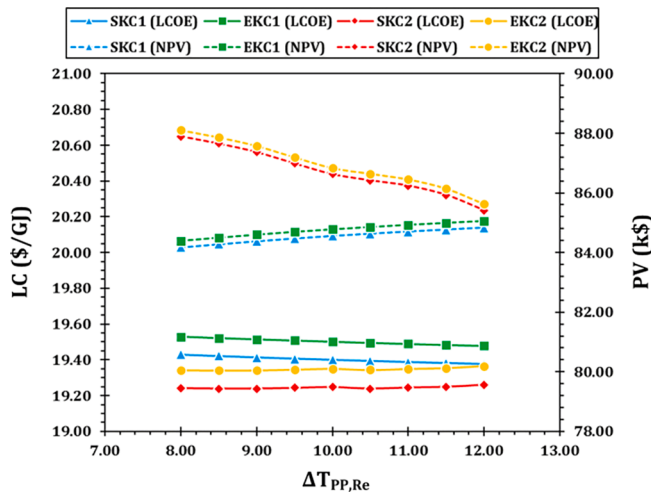
4.5.3. The effect of the variation of recuperators' pinch point temperature difference

Increasing the pinch point temperature difference of recuperators reduces the output temperature of cold streams in these heat exchangers, thereby decreasing the internal heat recovery quality of the cycles. However, the effect of this alteration on the net power capacity of KC2 is negative, while it is negligible on the power output of SKC1 and EKC1. According to the discussion in section 4.5.1, since the internal heat recovery system provided by recuperators is efficient in KC1, the whole thermal energy of the engine's exhaust gas is not utilized in the steam generator. So, increasing the pinch point temperature difference of recuperators makes the working fluid of KC1 obtain the excess thermal energy available in the engine's exhaust gas. In other words, making the recuperation less efficient by increasing the pinch point is compensated by more utilization of the exhaust gas. In contrast, in normal conditions, KC2 utilizes the maximum thermal capacity of the engine's exhaust gas, so when the demand for external energy increases because of the degradation of the internal heat recovery system by increasing the pinch point temperature difference, there would be no compensation capacity in the steam generator. Hence, the net power capacities of SKC2 and EKC2 decrease and make the energy and exergy efficiencies decline (see Figs. 18 and 19).

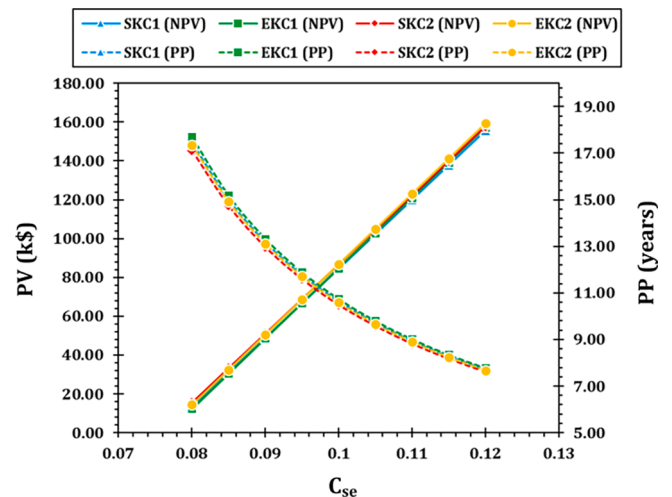It is also evident in Fig. 18 that the amount of avoided CO₂ by

Fig. 22. Variation of PV and PP with the variation of the unit price of electricity.

operating SKC2 and EKC2 would be reduced by about 0.9 kg/hr due to the variation of the recuperators' pinch point temperature difference from 8 to 12 K. The economic consequences of increasing the pinch point temperature difference of recuperators are illustrated in Fig. 20. The rise in this parameter leads to a reduction in the heat transfer areas of these heat exchangers. Therefore, the investment costs of recuperators are pulled down. The confrontation of this reduction with the decrease of the net power capacity in KC2 results in a slight upward trend for the LC of SKC2 and EKC2.

Adversely, since there is no reduction in the power capacity of KC1 imposed by the increment of pinch point temperature difference, the decline in investment costs of recuperators causes a slight downward trend in the LC of SKC1 and EKC1. The behavior of the PV diagram is precisely opposite of the diagrams of LC, however, with considerable variations in values.

4.5.4. The effect of the variation of the cycles' capacity factors

Increasing the capacity factor of Kalina cycles leads to an extension in their working hours, which means that more electricity will be produced and hence, more profit will be achieved. Therefore, value of PV augments by increasing the capacity factor from 0.72 to 0.88 in Fig. 21.

It is also worth noting that obtaining more profit during the working period of the Kalina cycles makes it earlier to pay all the costs associated with the establishment and maintenance of systems. Thus, the payback period will become shorter by increasing the capacity factor and thereby increasing the PV. The difference between Kalina cycles has been discussed in previous sections. Although it seems that the diagrams attributed to various Kalina cycles are almost coincident, the difference in the values of their PVs and PPs should be gained traction.

4.5.5. The effect of the variation of the unit price of electricity

According to Fig. 22, the net present value and payback period culminate with the increase in electricity price. The unit price of electricity sold to the grid can be varied during the time and locations where the systems are operating. So, studying the impact of the electricity selling price on the values of PV and PP is essential. Fig. 15 reveals that varying the unit price of electricity from 0.08 to 0.12 $\$/kWh$ causes PV to rise from 13.45, 12.27, 15.57, and 14.40 $k\$$ to 155.67, 157.28, 157.69, and 159.28 $k\$$, respectively for SKC1, EKC1, SKC2, and EKC2. Consequently, the payback period decreases from 17.46, 17.71, 17.11, and 17.35 years to 7.71, 7.78, 7.61, and 7.68 years, respectively, for SKC1, EKC1, SKC2, and EKC2. The trend of the payback period diagrams is convergent. The main reason behind this behavior is that even with increasing the selling profits, it takes time to make up the investment costs of the proposed systems, which possess the largest portion of all the costs associated with establishing the whole plant.

5. Conclusions

A comparative thermodynamic, economic, and environmental assessment is carried out on two well-known high-temperature Kalina cycles utilizing the waste heat of a Diesel engine's exhaust gas. The enhanced forms of these cycles were proposed by embedding the thermoelectric generators in the condensers of KCs. A self-optimization procedure has been considered for the energy modeling of four Kalina cycles (two simple and two integrated cycles) to achieve the maximum power output while locating the optimum pinch point in condensers. The *fmincon* solver of MATLAB was selected to conduct the optimization procedure, which took much shorter (5 to 8 min) to run the mathematical model of each cycle compared with other similar works. The decision variables of the optimization problem included the outlet pressure of the turbine (P_2), the temperature of the outlet stream of recuperator 1 (T_{10}), the ammonia mass fraction of the outlet stream of recuperator 1 (x_{10}), the pressure of condenser 2 (P_{15}), and the outlet temperature of the engine's exhaust gas from the steam generator (T_{HS2}). The main findings of this study are summarized as follows:

- The embedded TEGs could provide 0.29 to 0.82 kW power in enhanced Kalina cycles representing an efficiency of 0.66 to 1.03 %.
- The exergy assessments reveal that the steam generator and the turbine have the highest exergy destruction rates in all cycles.
- Comparing the performance criteria of four Kalina cycles in the optimized case, the enhanced KCs have a better performance from the environmental and thermodynamic viewpoints, even though this privilege was not considerable and significant. However, from the economic perspective, the enhanced cycles had more cost indicators (smaller profit indicators) than their equivalent simple structures. This difference was mild in TI and negligible in LC, PV, and PP.
- Increasing the ammonia mass fraction at the turbine inlet can improve the energy and exergy efficiencies of SKC1 and EKC1. Nevertheless, the increment of this parameter had negative impacts on the environmental and economic performance of all Kalina cycles, along with the energy and exergy efficiencies of SKC2 and EKC2. The turbine inlet pressure growth had desirable effects on all the performance criteria of four Kalina cycles. Increasing the pinch point temperature difference of recuperators had no considerable impact on the performance of SKC1 and EKC1, while it had a mild positive result from the economic point of view. On the other hand, increasing the pinch point temperature difference of recuperators causes a mild decline in all the performance indices of SKC2 and EKC2. The comparative investigation accomplished in the present work shows that the two proposed Kalina cycles have different advantages and disadvantages, which helps designers and engineers choose either KC1 structures or KC2 ones based on their working circumstances, restrictions, and requirements.
- Increasing the capacity factor and the unit price of electricity would result in improvements in the economic profits of all four cycles.

6. Discussion and future studies

One of the most important objectives of this study was to assess the energetic and economic profitability of embedding the TEGs in industrial WHR cycles such as Kalina. In this study, a comparative 4E evaluation of the advantages and disadvantages of the integration of TEGs with two well-known high-temperature Kalina cycles was conducted. Moreover, an unbiased discussion on the pros and cons of this integration and each Kalina cycle was provided as well. This makes scientific audiences and other researchers decide much easier on 1) which Kalina cycle can meet their demands while fitting their circumstances; 2) whether to use TEGs in their similar systems or not; This research reveals that the KC1 cycles are more efficient than KC2 cycles in energy and exergy perspectives, while the KC2 cycles are more cost-effective and profitable than KC1. Their environmental indices are almost the same in both simple and enhanced forms. Furthermore, although TEGs are simple and useful components that can operate even with low-temperature waste heat sources and improve the whole cycle's efficiency, their efficiency is too low to be embedded in all heat exchangers, especially in systems with high power generation capacities.

The life cycle assessment for more detailed environmental conclusions, along with the multi-objective optimization of the proposed cycles, are recommended to be implemented in future studies. The results of this research and those conducted in the future would assist researchers and industrial developers in decisively employing their desired Kalina cycle in the WHR systems.

CRediT authorship contribution statement

Arvin Sohrabi: Conceptualization, Methodology, Software, Validation, Writing – review & editing. **Nima Asgari:** Conceptualization, Methodology, Validation, Writing – original draft. **Muhammad Imran:** Supervision, Writing – review & editing. **Muhammad Wakil Shahzad:** Supervision, Writing – review & editing.
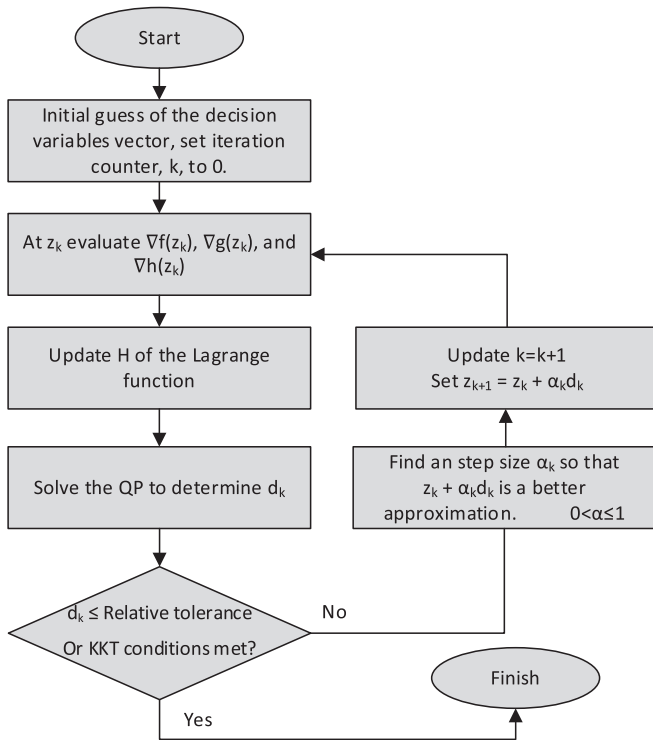
Fig. A1. The flowchart of the Sequential Quadratic Programming method.

interests or personal relationships that could have appeared to influence the work reported in this paper.

Data availability

Data will be made available on request.

Declaration of Competing Interest

The authors declare that they have no known competing financial

Appendix

Among the algorithms, which the MATLAB solver can use, the SQP (Sequential Quadratic Programming) was used in the current study since it showed faster performance than the other ones.

In fact, SQP is one of the best techniques for numerically solving constrained nonlinear optimization problems. It makes use of a strong theoretical underpinning and offers potent algorithmic tools for the resolution of significant technologically relevant problems on a large scale. SQP uses a linear approximation to resolve nonlinear issues. A quadratic subproblem is created using Newton's approach, which is simpler to solve [54,55]. Nonlinear optimization problems (NLP) of the following type are taken into consideration for the application of the SQP methodology [54]:

$$minimze\, f(z)\, over\, x \in \mathbb{R} \tag{A1}$$

Subject to:

$$g_i(z) = 0,\ i \in \mathbb{N} \tag{A2}$$

$$h_j(z) \le 0,\ j \in \mathbb{N} \tag{A3}$$

Here, f is the objective function. Also, g and h are the equality and inequality constraints, respectively. After initiating the solving process, the solver tries to find a reasonable point around the initial guess while assuring that no constraint is violated. First, the Lagrangian function of the problem is introduced:

$$L(z, \lambda, \mu) = f(z) + \lambda g(z)^T + \mu h(z)^T \tag{A4}$$

In this equation, λ and μ, respectively, are the vector of multipliers for equality and inequality. The constraints are linearized in order to construct the quadratic sub-problem, As shown in the following equations.

$$minimze\, \nabla f(z_k)^T d + \frac{1}{2}d^T Hf(z_k)d \tag{A5}$$

Subject to:

$$g_i(z_k) + \nabla g_i(z_k)^T \mathrm{d} = 0,\ i \in \mathbb{N} \tag{A6}$$

$$h_j(z_k) + \nabla h_j(z_k)^T \mathrm{d} \le 0,\ j \in \mathbb{N} \tag{A7}$$

The above equations are solved to yield a solution vector d and two multiplier vectors λ and μ, defined as $d = z - z_k$, $\Delta\lambda = \lambda - \lambda_k$, and $\Delta\mu = \mu - \mu_k$ respectively. This quadratic result determines the appropriate estimates for the Karush-Kuhn-Tucker (KKT) multipliers and H, as well as the search

direction for *x*. *H* is a positive definite Hessian matrix of the Lagrangian function. The Broyden-Fletcher-Goldfarb-Shanno method, which determines the second derivatives of the objective function and constraint functions, updates the value of *H*. When vector d is less than the relative tolerance and the KKT criteria are met, the solution converges. To guarantee the decline in the goal function, the step size is used. Finally, up until the solution z^* is attained, the technique outlined above is repeated. The whole process is summarized in Fig. A1 [55].

References

[1] Yoro KO, Daramola MO. Chapter 1 - CO2 emission sources, greenhouse gases, and the global warming effect. In: Rahimpour MR, Farsi M, Makarem MA, editors. Adv. Carbon Capture, Woodhead Publishing; 2020, p. 3–28. 10.1016/B978-0-12-819657-1.00001-3.

[2] Shu G, Liu L, Tian H, Wei H, Yu G. Parametric and working fluid analysis of a dual-loop organic Rankine cycle (DORC) used in engine waste heat recovery. Appl Energy 2014;113:1188–98. https://doi.org/10.1016/j.apenergy.2013.08.027.

[3] Keinath CM, Delahanty JC, Garimella S, Garrabrant MA. Compact Diesel Engine Waste-Heat-Driven Ammonia-Water Absorption Heat Pump Modeling and Performance Maximization Strategies. J Energy Resour Technol 2021:144. https://doi.org/10.1115/1.4051804.

[4] Usman M, Imran M, Yang Y, Lee DH, Park B-S. Thermo-economic comparison of air-cooled and cooling tower based Organic Rankine Cycle (ORC) with R245fa and R1233zde as candidate working fluids for different geographical climate conditions. Energy 2017;123:353–66. https://doi.org/10.1016/j.energy.2017.01.134.

[5] Zhu S, Zhang K, Deng K. A review of waste heat recovery from the marine engine with highly efficient bottoming power cycles. Renew Sustain Energy Rev 2020;120: 109611. https://doi.org/10.1016/j.rser.2019.109611.

[6] Costiuc I, Costiuc L, Radu S. Waste Heat Recovery Using Direct Thermodynamic Cycle. Bull Transilv Univ Brașov ● 2015;8:1–6.

[7] Lion S, Taccani R, Vlaskos I, Scrocco P, Vouvakos X, Kaiktsis L. Thermodynamic analysis of waste heat recovery using Organic Rankine Cycle (ORC) for a two-stroke low speed marine Diesel engine in IMO Tier II and Tier III operation. Energy 2019;183:48–60. https://doi.org/10.1016/j.energy.2019.06.123.

[8] Mohammadkhani F, Yari M. A 0D model for diesel engine simulation and employing a transcritical dual loop Organic Rankine Cycle (ORC) for waste heat recovery from its exhaust and coolant: Thermodynamic and economic analysis. Appl Therm Eng 2019;150:329–47. https://doi.org/10.1016/j.applthermaleng.2018.12.158.

[9] Jafarzad A, Asgari N, Ranjbar F, Mohammadkhani F. Thermodynamic assessment and optimization of the influences of the steam-assisted turbocharging and organic Rankine cycle on the overall performance of a diesel engine-based cogeneration integrated with a reverse osmosis desalination unit. Sustain Energy Technol Assessments 2021;46:101175. https://doi.org/10.1016/j.seta.2021.101175.

[10] Sohrabi A, Behbahaninia A, Sayadi S. Thermodynamic optimization and comparative economic analysis of four organic Rankine cycle configurations with a zeotropic mixture. Energy Convers Manag 2021;250:114872. https://doi.org/10.1016/j.enconman.2021.114872.

[11] Jouhara H, Khordehgah N, Almahmoud S, Delpech B, Chauhan A, Tassou SA. Waste heat recovery technologies and applications. Therm Sci Eng Prog 2018;6: 268–89. https://doi.org/10.1016/j.tsep.2018.04.017.

[12] Bombarda P, Invernizzi CM, Pietra C. Heat recovery from Diesel engines: A thermodynamic comparison between Kalina and ORC cycles. Appl Therm Eng 2010;30:212–9. https://doi.org/10.1016/j.applthermaleng.2009.08.006.

[13] Nemati A, Nami H, Ranjbar F, Yari M. A comparative thermodynamic analysis of ORC and Kalina cycles for waste heat recovery: A case study for CGAM cogeneration system. Case Stud Therm Eng 2017;9:1–13. https://doi.org/10.1016/j.csite.2016.11.003.

[14] Marami Milani S, Khoshbakhti Saray R, Najafi M. Comparison of different optimized heat driven power-cycle configurations of a gas engine. Appl Therm Eng 2020;179:115768. https://doi.org/10.1016/j.applthermaleng.2020.115768.

[15] Feng Y, Du Z, Shreka M, Zhu Y, Zhou S, Zhang W. Thermodynamic analysis and performance optimization of the supercritical carbon dioxide Brayton cycle combined with the Kalina cycle for waste heat recovery from a marine low-speed diesel engine. Energy Convers Manag 2020;206:112483. https://doi.org/10.1016/j.enconman.2020.112483.

[16] Ding P, Yuan Z, Shen H, Qi H, Yuan Ye, Wang X, et al. Exergoeconomic analysis and optimization of a hybrid Kalina and humidification-dehumidification system for waste heat recovery of low-temperature Diesel engine. Desalination 2020;496. https://doi.org/10.1016/j.desal.2020.114725.

[17] Mao Y, Zhang L, Wan L, Stanford RJ. Proposal and assessment of a novel power and freshwater production system for the heat recovery of diesel engine. Energy 2022; 240:122615. https://doi.org/10.1016/j.energy.2021.122615.

[18] Kalan AS, Ghiasirad H, Saray RK, Mirmasoumi S. Thermo-economic evaluation and multi-objective optimization of a waste heat driven combined cooling and power system based on a modified Kalina cycle. Energy Convers Manag 2021;247: 114723. https://doi.org/10.1016/j.enconman.2021.114723.

[19] Marston CH. Parametric Analysis of the Kalina Cycle. J Eng Gas Turbines Power 1990;112:107–16. https://doi.org/10.1115/1.2906464.

[20] Modi A, Haglind F. Thermodynamic optimisation and analysis of four Kalina cycle layouts for high temperature applications. Appl Therm Eng 2015;76:196–205. https://doi.org/10.1016/j.applthermaleng.2014.11.047.

[21] Sohrabi A, Behbahaninia A. Conventional and Advanced Exergy and Exergoeconomic Assessment of an Optimized System Consisting of Kalina and

[22] Mohammadkhani F, Yari M, Ranjbar F. A zero-dimensional model for simulation of a Diesel engine and exergoeconomic analysis of waste heat recovery from its exhaust and coolant employing a high-temperature Kalina cycle. Energy Convers Manag 2019;198:111782. https://doi.org/10.1016/j.enconman.2019.111782.

[23] Tohidi F, Ghazanfari Holagh S, Chitsaz A. Thermoelectric Generators: A comprehensive review of characteristics and applications. Appl Therm Eng 2022; 201:117793. https://doi.org/10.1016/j.applthermaleng.2021.117793.

[24] Mahmoudan A, Esmaeilion F, Hoseinzadeh S, Soltani M, Ahmadi P, Rosen M. A geothermal and solar-based multigeneration system integrated with a TEG unit: Development, 3E analyses, and multi-objective optimization. Appl Energy 2022; 308:118399. https://doi.org/10.1016/j.apenergy.2021.118399.

[25] Malik MZ, Musharavati F, Khanmohammadi S, Baseri MM, Ahmadi P, Nguyen DD. Ocean thermal energy conversion (OTEC) system boosted with solar energy and TEG based on exergy and exergo-environment analysis and multi-objective optimization. Sol Energy 2020;208:559–72. https://doi.org/10.1016/j.solener.2020.07.049.

[26] Nabat MH, Zeynalian M, Razmi AR, Arabkoohsar A, Soltani M. Energy, exergy, and economic analyses of an innovative energy storage system; liquid air energy storage (LAES) combined with high-temperature thermal energy storage (HTES). Energy Convers Manag 2020;226:113486. https://doi.org/10.1016/j.enconman.2020.113486.

[27] Zhang C, Shu G, Tian H, Wei H, Liang X. Comparative study of alternative ORC-based combined power systems to exploit high temperature waste heat. Energy Convers Manag 2015;89:541–54. https://doi.org/10.1016/j.enconman.2014.10.020.

[28] Zare V, Palideh V. Employing thermoelectric generator for power generation enhancement in a Kalina cycle driven by low-grade geothermal energy. Appl Therm Eng 2018;130:418–28. https://doi.org/10.1016/j.applthermaleng.2017.10.160.

[29] Malik MZ, Musharavati F, Khanmohammadi S, Pakseresht AH, Khanmohammadi S, Nguyen DD. Design and comparative exergy and exergo-economic analyses of a novel integrated Kalina cycle improved with fuel cell and thermoelectric module. Energy Convers Manag 2020;220:113081. https://doi.org/10.1016/j.enconman.2020.113081.

[30] Musharavati F, Khanmohammadi S, Pakseresht AH, Khanmohammadi S. Enhancing the performance of an integrated CCHP system including ORC, Kalina, and refrigeration cycles through employing TEG: 3E analysis and multi-criteria optimization. Geothermics 2021;89:101973. https://doi.org/10.1016/j.geothermics.2020.101973.

[31] Mosaffa AH, Hasani Mokarram N, Garousi FL. Thermoeconomic analysis of a new combination of ammonia/water power generation cycle with GT-MHR cycle and LNG cryogenic exergy. Appl Therm Eng 2017;124:1343–53. https://doi.org/10.1016/j.applthermaleng.2017.06.126.

[32] Cengel YA, Boles MA, Kanoğlu M. Thermodynamics: an engineering approach. 5th ed. New York: McGraw-Hill; 2011.

[33] Sohrabi A, Behbahaninia A, Sayadi S, Banifateme M. Advanced Exergy-Based Audit of Heat Recovery Steam Generators: A Case Study. J Energy Resour Technol 2022; 144. https://doi.org/10.1115/1.4052467.

[34] Bejan A, Tsatsaronis G, Moran MJ. Thermal design and optimization. John Wiley & Sons; 1996.

[35] Champier D. Thermoelectric generators: A review of applications. Energy Convers Manag 2017;140:167–81. https://doi.org/10.1016/j.enconman.2017.02.070.

[36] Snyder GJ, Toberer ES. Complex thermoelectric materials. Mater Sustain Energy A Collect Peer-Reviewed Res Rev Artic from Nat Publ Gr 2010:101–10. https://doi.org/10.1142/9789814317665_0016.

[37] Vorobiev Y, González-Hernández J, Vorobiev P, Bulat L. Thermal-photovoltaic solar hybrid system for efficient solar energy conversion. Sol Energy 2006;80: 170–6. https://doi.org/10.1016/j.solener.2005.04.022.

[38] Zhang X, He M, Zhang Y. A review of research on the Kalina cycle. Renew Sustain Energy Rev 2012;16:5309–18. https://doi.org/10.1016/j.rser.2012.05.040.

[39] Tsatsaronis G. Thermoeconomic analysis and optimization of energy systems. Prog Energy Combust Sci 1993;19:227–57. https://doi.org/10.1016/0360-1285(93)90016-8.

[40] Asim M, Saleem S, Imran M, Leung MKH, Hussain SA, Miró LS, et al. Thermo-economic and environmental analysis of integrating renewable energy sources in a district heating and cooling network. Energy Effic 2020;13(1):79–100.

[41] Asgari N, Khoshbakhti Saray R, Mirmasoumi S. Seasonal exergoeconomic assessment and optimization of a dual-fuel trigeneration system of power, cooling, heating, and domestic hot water, proposed for Tabriz. Iran Renew Energy 2023; 206:192–213. https://doi.org/10.1016/j.renene.2023.02.028.

[42] Lazzaretto A, Tsatsaronis G. SPECO: A systematic and general methodology for calculating efficiencies and costs in thermal systems. Energy 2006;31:1257–89. https://doi.org/10.1016/j.energy.2005.03.011.

[43] Tashtoush B, Morosuk T, Chudasama J. Exergy and Exergoeconomic Analysis of a Cogeneration Hybrid Solar Organic Rankine Cycle with Ejector. Entropy 2020;22 (6):702.

Organic Rankine Cycles for Waste Heat Recovery. J Energy Resour Technol 2022: 144. https://doi.org/10.1115/1.4054178.

[44] Ghiasirad H, Asgari N, Khoshbakhti Saray R, Mirmasoumi S. Thermoeconomic assessment of a geothermal based combined cooling, heating, and power system, integrated with a humidification-dehumidification desalination unit and an absorption heat transformer. Energy Convers Manag 2021;235:113969. https://doi.org/10.1016/j.enconman.2021.113969.

[45] Fan G, Dai Y. Thermo-economic optimization and part-load analysis of the combined supercritical CO2 and Kalina cycle. Energy Convers Manag 2021;245:114572. https://doi.org/10.1016/j.enconman.2021.114572.

[46] Bahrampoury R, Behbahaninia A. Thermodynamic optimization and thermoeconomic analysis of four double pressure Kalina cycles driven from Kalina cycle system 11. Energy Convers Manag 2017;152:110–23. https://doi.org/10.1016/j.enconman.2017.09.046.

[47] Javad DM. Enhancing energo-exergo-economic performance of Kalina cycle for low- to high-grade waste heat recovery: Design and optimization through deep learning methods. Appl Therm Eng 2021;195:117221. https://doi.org/10.1016/j.applthermaleng.2021.117221.

[48] Campos Rodríguez CE, Escobar Palacio JC, Venturini OJ, Silva Lora EE, Cobas VM, Marques dos Santos D, et al. Exergetic and economic comparison of ORC and Kalina cycle for low temperature enhanced geothermal system in Brazil. Appl Therm Eng 2013;52(1):109–19.

[49] Javanshir N, Seyed Mahmoudi SM, Rosen MA. Thermodynamic and Exergoeconomic Analyses of a Novel Combined Cycle Comprised of Vapor-Compression Refrigeration and Organic Rankine Cycles. Sustainability 2019;11 (12):3374.

[50] Georgousopoulos S, Braimakis K, Grimekis D, Karellas S. Thermodynamic and techno-economic assessment of pure and zeotropic fluid ORCs for waste heat recovery in a biomass IGCC plant. Appl Therm Eng 2021;183:116202. https://doi.org/10.1016/j.applthermaleng.2020.116202.

[51] Kolahi M, Yari M, Mahmoudi SMS, Mohammadkhani F. Thermodynamic and economic performance improvement of ORCs through using zeotropic mixtures: Case of waste heat recovery in an offshore platform. Case Stud Therm Eng 2016;8:51–70. https://doi.org/10.1016/j.csite.2016.05.001.

[52] Boyaghchi FA, Molaie H. Advanced exergy and environmental analyses and multi objective optimization of a real combined cycle power plant with supplementary firing using evolutionary algorithm. Energy 2015;93:2267–79. https://doi.org/10.1016/J.ENERGY.2015.10.094.

[53] Pardo Martínez CI. Energy and sustainable development in cities: A case study of Bogotá. Energy 2015;92:612–21. https://doi.org/10.1016/j.energy.2015.02.003.

[54] Boggs PT, Tolle JW. Sequential Quadratic Programming. Acta Numerica 1995;4:1–51.

[55] Aji SS, Kim YS, Ahn KY, Lee YD. Life-Cycle Cost Minimization of Gas Turbine Power Cycles for Distributed Power Generation Using Sequential Quadratic Programming Method. Energies 2018;11:3511. https://doi.org/10.3390/en11123511.